THE UNIVERSITY OF MANITOBA

NONLINEAR SCATTERING BY A POLYCONDUCTOR SLAB

by

Essam E.M. Hassan

A THESIS

SUBMITTED TO THE FACULTY OF GRADUATE STUDIES

IN PARTIAL FULFILMENT OF THE REQUIREMENTS FOR THE DEGREE

OF MASTER OF SCIENCE IN ELECTRICAL ENGINEERING

DEPARTMENT OF ELECTRICAL ENGINEERING

WINNIPEG, MANITOBA

May 1974

NONLINEAR SCATTERING BY A POLYCONDUCTOR SLAB

by

Essam E.M. Hassan

A dissertation submitted to the Faculty of Graduate Studies of the University of Manitoba in partial fulfillment of the requirements of the degree of

Master of Science

To my parents

with deep gratitude

ABSTRACT

A solution of the nonlinear electro-thermal problem of the scattering of plane electromagnetic waves normally incident on a poly-conductor slab with a metal substrate is presented. Since the electrical conductivity of the slab is a nonlinear function of the temperature profile, and hence the power absorbed at every point in the slab, the formulation for the electric field and temperature distribution in the slab leads to a pair of coupled nonlinear second order ordinary differential equations which are solved partially analytically by the W.K.B. method and partially numerically by the finite difference method.

The variations of the reflection coefficient, the surface impedance and surface temperature with frequency and incident electric field, as well as the resulting profiles of the electric field, conductivity and temperature inside the slab are presented in graphical form, discussed and analyzed. These results suggest certain practical applications which are also described.

ACKNOWLEDGEMENT

I wish to express my sincere appreciation to Dr. M.A.K. Hamid for his guidance and encouragement throughout this work. I am also grateful to my friends and colleagues for their discussions and suggestions and to Mrs. B. Glowasky who carefully and expertly typed the manuscript.

The financial support provided by Manitoba Research Council, Manitoba Hydro, and the Defence Research Board of Canada Grant 3801-42 is highly appreciated.

TABLE OF CONTENTS

CHAPTER PAGE

LIST OF FIGURES

FIGURE PAGE

1, INTRODUCTION

The problem of nonlinear scattering of electromagnetic waves from surfaces whose characteristics are not constant but are functions of the excitation or of the spatial coordinates is of great interest to the electrical engineer. Such a problem frequently occurs in the study of microwave heating processes or in analyzing the propagation of electromagnetic waves through plasma layers or along the surface of the earth where both the electrical parameters (e.g. permittivity, permeability, conductivity, etc.) and the physical parameters (such as temperature, viscosity, density, etc.) are dependent on the energy absorbed and hence on the field excitation. An example illustrating this is the problem of microwave heating of dielectrics where the material permittivity changes with excitation (e.g. moisture evaporation of food in a microwave oven where the real and imaginary parts of the permittivity change [1]) and where such variation is important in optimizing a microwave heating process in real time.

Due to the extreme difficulties encountered in the mathematical analysis of such a class of nonlinear problem, very little is known in this area. Most of the previous works have mainly dealt with the propagation of electromagnetic waves along the surface of the earth or through the layers of the atmosphere where in general the wave number of the medium is considered a function of the coordinates and not of the excitation; hence the interaction between the parameters and the excitation was not taken into account. Several problems where the wave number profiles allow the solutions to be expressed in a closed form have been investigated. The exponentially increasing conductivity with depth has been introduced by Shmoys in an anlysis for horizontally polarized waves

where he obtained a solution of the field in terms of the Hankel functions [2]. Galejs working on the same problem analyzed the case of vertical polarization where he again ended with a solution of the field in terms of the modified Bessel functions [3]. Another profile which leads to a convenient solution for the horizontal polarization is the linear variation of the wave number with depth leading to a solution in terms of the Airy functions [4]. Lahiri and Price analyzed the power law variation of the wave number with depth for the case of normal incidence, and again the resulting solution is in terms of Bessel functions, Hankel functions or power series depending on the assumed parameters [5]. An excellent discussion of these cases and several others has been reported by Wait [4].

It is seen that these investigations have dealt with special hypothetical profiles of the electrical parameters to allow for known tabulated solutions, yet the problem of the interdependence of these parameters and the excitation has not been investigated. It is the fundamental object of this research to study the nonlinear response of certain materials as their basic electrical and physical parameters change with excitation and the mechanisms of interaction between these parameters. The example singled out in this thesis specifically involves variations of the conductivity rather than the permittivity with excitation. A convenient material for this study is vanadium dioxide whose conductivity versus excitation characteristic has already been employed at D.C. and low A.C. frequencies to construct the so called MOXIE devices [6].

Vanadium dixoide is from a class of materials known as transition-to-metal polyconductors which at present and since the early work of Morin are the focus of considerable theoretical and experimental

efforts in order to investigate and explain their optical, thermal, electronic, nuclear and acoustic characteristics [7]-[12]. These materials are characterized by an exponential variation of the resistivity with the reciprocal of the absolute temperature [10]. They undergo a sudden transition at a specific temperature within a very small temperature range from a high resistivity semiconductor state at the lower temperatures to a low resistivity metallic behaviour at the higher temperatures due to a sudden change in their crystalline structure [7]-[8]. A polyconductor material experiences such a change by permitting external joule heating either directly through an external voltage source or indirectly by any source of heat in contact with it.

The characteristics of vanadium dioxide when directly heated by D.C., low frequency A.C. or rectangular voltage pulses through a pair of electrodes attached to it are well investigated. These characteristics include the response time (i.e. the time required for the device to switch after power is applied), the recovery time, the necessary conditions for initiation of switching, the switching energy and other several electric and physical properties [13]-[16]. However no attempt has yet been made to analyze these characteristics at microwave frequencies.

In this thesis an attempt is made to characterize this material shaped in the form of a slab deposited on a metal substrate at microwave frequencies where microwave power is used for excitation. This type of assembly is so chosen since usually vanadium dioxide is deposited on a metal backing.

It is obvious that when electromagnetic waves are incident on a vanadium dioxide slab, part of the power may be absorbed in the medium and the remainder reflected back according to the value of the reflection

coefficient at the surface. However the reflection coefficient is dependent on the interaction between the parameters of the medium and the excitation, thus in order to clearly define the problem, it is necessary to classify the various variables as dependent or independent in the subsequent mathematical analysis. We note from simple physical reasoning that part of the incident power is absorbed and hence affects the temperature. Once the temperature rises above room temperature, the material conductivity appears to increase, at least in the low frequency case of constant excitation, thus affecting the reflection coefficient and the amount of power absorbed. As the power absorption decreases for higher conductivities, the material scatters like a conductor until it cools to the point where its conductivity decreases and power is absorbed again, and the cycle repeats. Because of the complex analysis involved, only that part of this cycle related to increasing conductivity, where the reflection coefficient approaches unity is presented. The complete analysis and film behaviour can be derived from the solution presented here although further analysis of certain effects (e.g. hysterisis, delay and recovery time, etc.) into the complete cycle is obviously desirable but will be left for future investigation after the appropriate mathematical tools are developed and experimental data is obtained.

According to the previous discussion, mathematical formulation of the problem in the nonlinear polyconductor medium results in two coupled nonlinear second order ordinary differential equations in the temperature and the electric field. To solve a nonlinear ordinary differential equation, several techniques such as converting it into an integral equation or using the perturbation technique are available. In both

cases iterative solutions leading to a few terms of a series solution may be found. However, due to the coupling between both equations under consideration, and the nonlinear nature involved, finding a solution, even numerically, may be very difficult since the starting function of one of the variables to initiate the solution (which is very likely far from the correct solution) will directly affect the starting function of the other variable, and hence no guarantee of convergence is at hand. The method adopted here is based on decoupling the two equations using the W.K.B. method which results in one nonlinear ordinary differential equation in only one unknown whose numerical solution is easier than the previous case. The formulation of the nonlinear problem is described in Chapter 2, and the method adopted in the solution for both the electric field and the temperature are presented in Chapter 3. In Chapter 4 the results are discussed and analyzed, and a number of possible improvements and extensions of the theoretical analysis are suggested for future research. Finally some proposals regarding Moxie-like devices which operate at microwave frequencies for various instrumentational purposes are suggested in Chapter 5.

2. FORMULATION OF THE NONLINEAR SCATTERING PROBLEM

In this chapter we consider formulating the nonlinear scattering by a polyconductor slab on a metal substrate taking into account heat conduction and the nonlinear nature of the electrical conductivity of the slab with the incident electromagnetic power.

2.1 Statement of the problem and objectives

Consider an infinite polyconductor slab on a metal substrate as shown in Figure (2.1). Let the polyconductor occupy region II ($0 < z < h$), the substrate occupy region III ($h < z < \infty$) and free space occupy region I ($z < 0$). Also assume a plane wave incident from region I at angle $\theta = \theta_o$ on the slab with a y-polarized electric field given by

$$E^i = E_o \exp(-j K_o z \cos\theta_o - j K_o x \sin\theta_o) \tag{2.1}$$

where $e^{j\omega t}$ time dependence has been suppressed and $K_o = \omega\sqrt{\mu_o \varepsilon_o}$ is the free space wave number.

The scattered field in region I is also y-polarized and may be expressed in the form

$$E^s = R(E_o)\, E_o \exp(j K_o z \cos\theta_o - j K_o x \sin\theta_o) \tag{2.2}$$

where the reflection coefficient $R(E_o)$ is a function of the incident field as well as of the slab thickness.

The Leontovich impedance boundary condition at the interface between the free space and the polyconductor slab requires that the total fields at the boundaries be related as [17]

$$\vec{E} - (\hat{n} \cdot \vec{E})\hat{n} = Z_s\,(E_o)(\hat{n} \times \vec{H}) \tag{2.3}$$

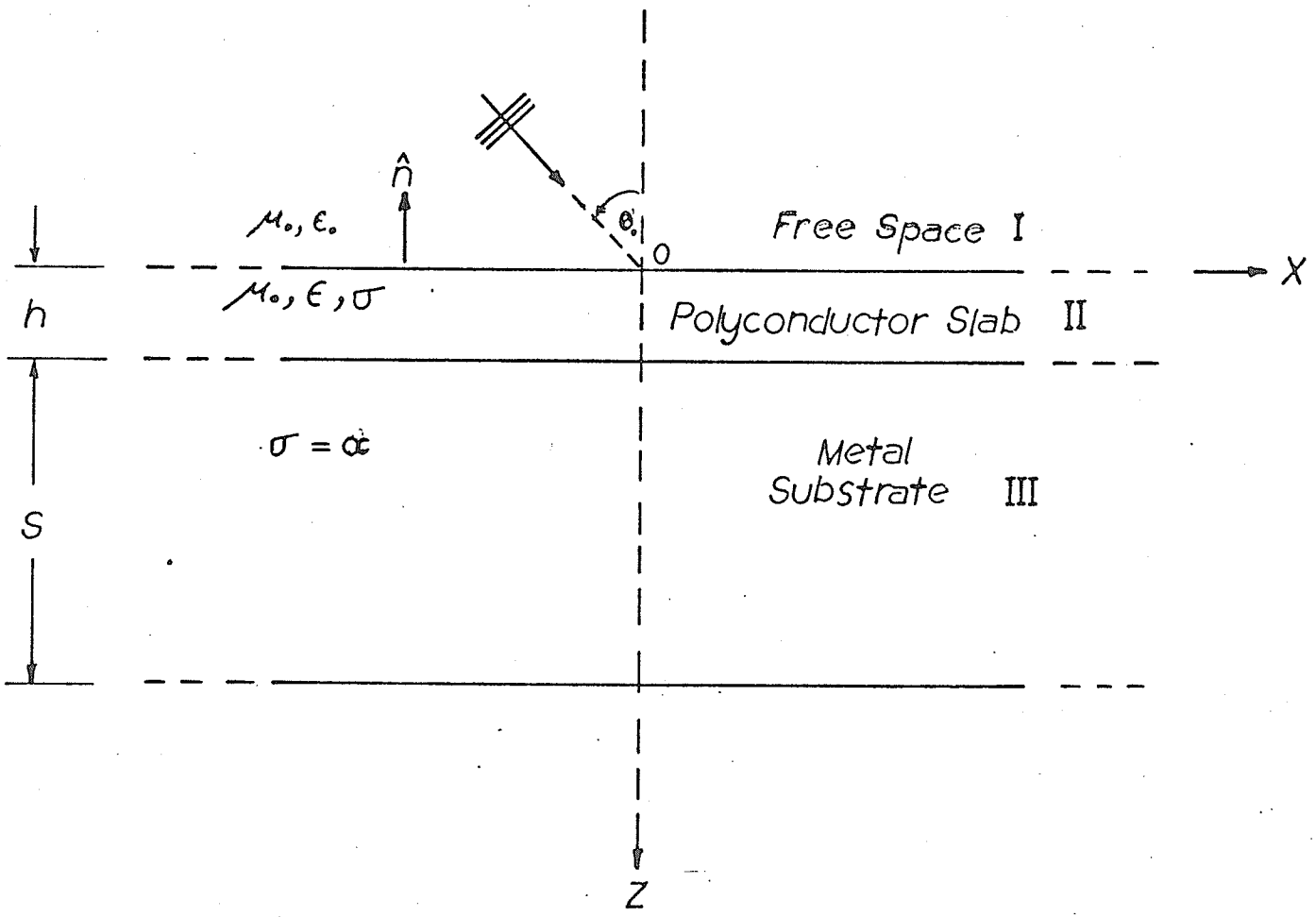

Fig. 2.1 Scattering geometry for the polyconductor assembly

where $Z_s(E_o)$ is the effective surface impedance considered to be a function of the incident electric field, $\vec{E}$ and $\vec{H}$ are the total electric and magnetic fields at the interface respectively, and $\hat{n}$ denotes the unit outward normal as shown in figure (2.1).

Application of (2.3) at the surface $z = 0$ leads to:

$$E_y = -Z_s(E_o)\, H_x \tag{2.4}$$

The x-component of Maxwell's equation

$$\nabla \times \vec{E} = -\frac{\partial \vec{B}}{\partial t} \tag{2.5}$$

gives

$$\frac{\partial E}{\partial z} = j\omega\mu\, H_x \tag{2.6}$$

Hence, using (2.6), (2.2) and (2.1) we obtain

$$-j\, K_o \cos\theta_o [E_o \exp(-j\, K_o\, z \cos\theta_o) - R(E_o)\, E_o \exp(j\, K_o\, z \cos\theta_o)]$$

$$\cdot \exp(-j\, K_o\, x \sin\theta_o) = j\omega\, \mu_o\, H_x$$

and thus

$$H_x = -\frac{K_o \cos\theta_o}{\omega\, \mu_o} E_o \exp(-j\, K_o\, x \sin\theta_o)[\exp(-j\, K_o\, z \cos\theta_o) - R(E_o) \cdot \exp(j\, K_o\, z \cos\theta_o)] \tag{2.7}$$

Substituting (2.1) and (2.2) in (2.4) gives

$$E_o \exp(-j\, K_o\, x \sin\theta_o)[\exp(-j\, K_o\, z \cos\theta_o) + R(E_o)\exp(j\, K_o\, z \cos\theta_o)] = Z_s(E_o) \frac{K_o \cos\theta_o}{\omega\, \mu_o} \cdot E_o \exp(-j\, K_o\, x \sin\theta_o) \cdot [\exp(-j\, K_o\, z \cos\theta_o) - R(E_o) \exp(j\, K_o\, z \cos\theta_o)] \tag{2.8}$$

at the interface $z = 0$. Equation (2.8) hence becomes

$$Z_s(E_o) \cdot \frac{K_o \cos\theta_o}{\omega \mu_o} \cdot [1 - R(E_o)] = 1 + R(E_o) \qquad (2.9)$$

Solving for $R(E_o)$ yields

$$R(E_o) = [Z_s(E_o) - (\eta_o/\cos\theta_o)]/[Z_s(E_o) + (\eta_o/\cos\theta_o)] \qquad (2.10)$$

where $\eta_o = \sqrt{\mu_o/\varepsilon_o}$ is the free space intrinsic impedance.

Thus the problem reduces to finding the surface impedance evaluated at the interface $z = 0$. In other words, the wave equation has to be derived as shown in the next section and solved as shown in a later section.

2.2 Wave equation in polyconductor slab

The electric field in region II may be assumed to have an x variation in the form $\exp(-j\, K_o\, x\, \sin\theta_o)$ in order that the tangential field components be matched for all values of x along the upper interface $z = 0$. Since the field is also a function of z, we assume the form

$$E^t = E(z)\, \exp(-j\, K_o\, x\, \sin\theta_o) \qquad (2.11)$$

where the transmitted field component E^t must satisfy the vector wave equation

$$\nabla^2 \vec{E} = \mu\sigma \frac{\partial \vec{E}}{\partial t} + \mu\varepsilon \frac{\partial^2 \vec{E}}{\partial t^2} \qquad (2.12)$$

Here, μ, ε and σ are the permeability, permittivity and conductivity of the polyconductor medium, respectively.

Substitution of (2.11) into (2.12) gives

$$\frac{d^2\vec{E}(z)}{dz^2} - K_o^2 \sin^2\theta_o \, E(z) = (j\omega\mu\sigma - \omega^2\mu\varepsilon) \, E(z) \qquad (2.13)$$

Letting $\varepsilon = \varepsilon_o\varepsilon_r$, where ε_o is the free space permittivity and ε_r is the complex relative dielectric constant, i.e.,

$\varepsilon_r = \varepsilon_r' - j\varepsilon_r''$, equation (2.13) takes the form

$$\frac{d^2E(z)}{dz^2} + (\omega^2\mu \, \varepsilon_o\varepsilon_r' - K_o^2 \sin^2\theta_o) \, E(z) - j\omega\mu(\sigma + \omega\varepsilon_o\varepsilon_r'') \, E(z) = 0 \qquad (2.14)$$

In the special case of the Vanadium dioxide (VO_2) polyconductor under consideration, the resistivity is reported to exhibit nearly an approximately exponential dependence on the reciprocal of the absolute temperature over a wide temperature range [10]. Accordingly, the conductivity may be written in the form

$$\sigma = \sigma_o \exp(-F/T_K) \qquad (2.15)$$

where

$F = \Delta E/K_p$

ΔE = activation energy of the polyconductor.

K_p = Boltzman's constant (1.3806×10^{-23} joule/°K).

T_K = Absolute temperature in degrees Kelvin.

σ_o = constant.

It is shown in Appendix A that (2.15) can be rewritten in the form

$$\sigma = \sigma(T_a) \exp\{\beta \cdot T/(1 + T/T_a)\} \qquad (2.16)$$

where

T_a = reference temperature in °K.

T = temperature rise above T_a in °K.

$\beta = F/T_a^2$

Equation (2.14) hence takes the form

$$\frac{d^2E(z)}{dz^2} + [K_o^2 (\varepsilon_r' - \sin^2\theta_o) - j\omega\mu\{\sigma(T_a) \exp[\beta T/(1 + T/T_a)] + \omega \varepsilon_o \varepsilon_r''\}] E(z) = 0 \qquad (2.17)$$

which is a second order ordinary differential equation in two unknowns, the electric field and the temperature. A complete solution of (2.17) requires more information about the temperature distribution inside the slab which in turn requires analysis of the electrothermal balance throughout the polyconductor region.

2.3. Heat conduction

It is shown that to complete the solution of the problem, the thermal balance at every point inside the slab must be analyzed. Since the polyconductor slab is thermally in the solid state condition where heat transfer takes place by conduction, the problem of heat conduction in solids have to be analyzed. In the following section the general problem of heat conduction will be reviewed first, then the special case of the polyconductor slab will be dealt with in the next section.

2.3.1. *Heat conduction in solids*

Heat transfer by conduction takes place in both solids and fluids provided that temperature differences exist. The mathematical theory of heat conduction treats matter as being continuous and is based

on a generalized macroscopic analysis of energy transfer in a solid. According to such theory, if heat is produced in a solid so that at a point $P(x,y,z)$ heat is supplied at rate $q(x,y,z,t)$ per unit time per unit volume, then [18]

$$\frac{\partial}{\partial x}\left(k\,\frac{\partial T}{\partial x}\right) + \frac{\partial}{\partial y}\left(k\,\frac{\partial T}{\partial y}\right) + \frac{\partial}{\partial z}\left(k\,\frac{\partial T}{\partial z}\right) + q = C\rho\,\frac{\partial T}{\partial t} \tag{2.18}$$

where

k = thermal conductivity of the solid

C = specific heat

ρ = density of the medium.

If k does not vary with temperature, but the medium is heterogeneous or homogeneous but anisotropic equation (2.18) becomes

$$k_x\,\frac{\partial^2 T}{\partial x^2} + k_y\,\frac{\partial^2 T}{\partial y^2} + k_z\,\frac{\partial^2 T}{\partial z^2} + q = C\rho\,\frac{\partial T}{\partial t}$$

while if k is constant and the medium is homogeneous equation (2.18) becomes

$$k\,\nabla^2 T + q = C\rho\,\frac{\partial T}{\partial t} \tag{2.19}$$

The thermal conductivities of solids generally vary slowly with temperature, hence equation (2.19) is frequently used in practice using the average value of k within the small temperature range of practical interest. This usually leads to reasonably satisfactory results for the required degree of accuracy in practice. The averaging procedure will be one of the assumptions when formulating and solving the problem of heat conduction in a VO_2 region as shown in the following section.

2.3.2. *Heat conduction in polyconductor slab*

In analyzing the problem of electothermal balance in the VO_2 region, the following assumptions are made:

i) The medium is thermally homogeneous as long as the temperature difference between the upper and the lower surfaces is within a few degrees compared to the temperature of either surface.

ii) For a thermally homogeneous medium the thermal conductivity is assumed constant and equal to its average value across the slab.

We may show that this is justified as long as the variation of k with T is slow [18] such that

$$\frac{1}{k_a}\int_{T_o}^{T+T_o} k\, dT \simeq T \tag{2.20}$$

where k_a is the average value of the thermal conductivity in the temperature range T_o to T. Assume that

$$\theta = \frac{1}{k_a}\int_{T}^{T+T_o} k\, dT \tag{2.21}$$

therefore

$$\frac{\partial\theta}{\partial X} = \frac{k}{k_a}\frac{\partial T}{\partial X}\ ;\quad \frac{\partial\theta}{\partial y} = \frac{k}{k_a}\frac{\partial T}{\partial y}\ ;\quad \frac{\partial\theta}{\partial z} = \frac{k}{k_a}\frac{\partial T}{\partial z}$$

Hence

$$\frac{\partial}{\partial z}\left(k\frac{\partial T}{\partial z}\right) = k_a\frac{\partial}{\partial z}\left(\frac{\partial\theta}{\partial z}\right) = k_a\frac{\partial^2\theta}{\partial z^2}$$

which is also true for the other two derivatives over x and y.

Equation (2.18) for steady state condition becomes

$$k_a\nabla^2\theta + q = 0 \tag{2.22}$$

Since the only source of heat in the slab is the power dissipated at each point of the medium due to the portion of the incident electromagnetic power transmitted through it, the term q in (2.22) is readily given by [19].

$$q = \mathrm{Re} \cdot \{\hat{y} \cdot |E|^2\} \tag{2.23}$$

where

$$\begin{aligned}\hat{y} &= \sigma + j\omega\varepsilon \\ &= \sigma + j\omega\varepsilon_o (\varepsilon_r' - j\varepsilon_r'') \\ &= (\sigma + \omega\varepsilon_o \varepsilon_r'') + j\omega\varepsilon_o\varepsilon_r'\end{aligned}$$

then (2.23) is rewritten as

$$q = (\sigma + \omega\varepsilon_o\varepsilon_r') \ |E(z)|^2$$

and equation (2.22) representing the steady state conduction of heat in the polyconductor slab is expressed as

$$k_a \nabla^2\theta + [\sigma(T_a) \exp\{\beta T/(1 + T/T_a)\} + \omega\varepsilon_o\varepsilon_r''] \cdot |E(z)|^2 = 0 \tag{2.24}$$

Using (2.20) and (2.21), we have

$$\theta \simeq T$$

from which (2.24) becomes

$$k_a \nabla^2 T + [\sigma(T_a) \exp\{\beta T/(1 + T/T_a)\} + \omega\varepsilon_o\varepsilon_r''] \cdot |E(z)|^2 = 0 \tag{2.25}$$

Since the magnitude of the electric field $E(z)$ is a function of z only, the power dissipated at all points on a constant z plane

is the same. Accordingly there will be no temperature gradient in the lateral directions, and equation (2.22) can hence be further simplified to

$$k_a \frac{d^2T}{dz^2} + [\sigma(T_a) \exp\{\beta \cdot T/(1 + T/T_a)\} + \omega\varepsilon_o\varepsilon_r''] \, |E(z)|^2 = 0 \tag{2.26}$$

Equations (2.17) and (2.26) are two coupled differential equations in $E(z)$ and $T(z)$. We seek their solution simultaneously subject to appropriate boundary conditions to be discussed in some detail in the subsequent sections.

2.4. Boundary conditions

The boundary conditions involved in this problem are apparently of two distinguished types: the electromagnetic boundary and the thermal boundary conditions.

In spite of the special nature of this problem, the electromagnetic field boundary conditions will still hold in their most general form, that is the tangential component of the electric field and the normal component of the magnetic field are continuous at the boundaries. The Leontovitch boundary conditions in fact introduces a relation between the tangential component of the electric field and the discontinuous tangential component of the magnetic field at surface of discontinuity in case of a imperfectly conducting surface and thus they replace the exact boundary conditions, hence permitting considerable simplification of many scattering and diffraction problems dealing with electromagnetic waves.

Determinination of the electromagnetic boundary conditions will be the subject of the following section. Formulas governing the thermal

boundary conditions will be derived in the next section.

2.4.1. *Electromagnetic boundary conditions*

Since the magnetic field does not appear in any of the two differential equations (2.17) and (2.26), we will only discuss the boundary conditions imposed on the electric field. It is well known that, the transition of the tangential components of the vector $\vec{E}$ through a surface of discontinuity is continuous. Mathematically this is expressed as

$$\hat{n} \times (E_2 - E_1) = 0 \tag{2.27}$$

where E_1 is the field in one medium, E_2 is the field in the other medium all evaluated at the surface of discontinuity and $\hat{n}$ is the outward normal pointing from the second medium to the first (i.e. negative z direction in Figure 1).

Applying (2.27) at the interface $(z = 0)$ between medium I and medium II immediately gives

$$E^i + E^S = E^t \tag{2.28}$$

using equations (2.1), (2.2) and (2.11) in (2.28) yields

$$E(0) = E_o[1 + R(E_o)] \tag{2.29}$$

which determines the relation between the transmitted and incident fields at the surface of discontinuity.

Again applying (2.27) at the interface between medium II and medium III gives

$$E(h) = 0 \tag{2.30}$$

Since the electric field transmitted to medium III is zero due to its assumed infinite conductivity.

Equations (2.29) and (2.30) represent the two boundary conditions to be satisfied by the electric field to complete the solution.

2.4.2. *Thermal boundary conditions*

The surface conditions usually arising in the mathematical theory of heat are of several types, however we will limit the discussion to only two cases describing the conditions of the surfaces $z = 0$ and $z = h$.

At the interface $z = 0$ the slab surface will emit heat to the surrounding through radiation according to the relation [18]

$$k_a \left.\frac{dT}{dn}\right|_{z=0} + \delta\, \varepsilon[(T_S + T_a)^4 - T_a^4] = 0 \qquad (2.31)$$

where:

T_S = temperature of upper surface of the slab above T_a

ε = emmissivity of the surface

δ = Stefan-Boltzman constant

Equation (2.31) can be further simplified to

$$k_a \left.\frac{dT}{dn}\right|_{z=0} + 4\delta\, \varepsilon\, T_a^3\, T_S = 0 \qquad (2.32)$$

provided that $T/T_a << 1$.

At the interface $z = h$ the slab surface will transmit heat by conduction through the substrate. Hence [18]

$$k_a \left.\frac{dT}{dn}\right|_{z=h} + \frac{K_S}{S} \cdot T_h = 0 \qquad (2.33)$$

where

T_h = temperature of the lower surface of the slab above T_a

S = depth of the substrate

K_S = thermal conductivity of the substrate.

Once the solution for the electric field and temperature is found from equations (2.17) and (2.26) for a given transmitted field, the magnetic field is determined using equation (2.6), and the surface impedance is finally evaluated from equation (2.4). With the aid of equation (2.10) the reflection coefficient can also be determined leading to the incident electric field from (2.29). This is the subject of the following chapter.

3. APPROXIMIATE SOLUTION OF THE PROBLEM

Chapter 2 has dealt with the formulation of the nonlinear scattering problem which results in a pair of coupled nonlinear partial differential equations as already shown. Several methods are available for approximating the solution of a nonlinear ordinary differential equation, however they generally follow the same general procedure of assuming a physically reasonable solution for the differential equation then improving it by successive iterations. Here, due to the coupling between the two differential equations, finding simultaneously two convergent series solutions for the electric field and the temperature may be very difficult. Hence it is advantageous to decouple the two differential equations in question and solve for both the unknowns independently. In an attempt to decouple these equations we seek an approximate solution for the electric field [from equation (2.17)] in terms of the temperature using the W.K.B. method, then we proceed to substitute in (2.26) to complete the solution as will be shown in the following sections.

The Jeffreys or Wentzel-Kramers-Brillouin method is a technique for finding an approximate solution to the second order differential equation of the form

$$\frac{d^2W}{dz^2} + f(z) \cdot W = 0 \tag{3.1}$$

throughout a region R in which $f(z)$ is analytic and contains no zeros, with the restriction that $f(z)$ varies very slowly [20].

The W.K.B. approximate solution of (3.1) may be written in the form

$$W(z) = f^{\frac{1}{4}}(z) \cdot \{A \exp[j\ F(z)] + B \exp[-j\ F(z)]\} \tag{3.2}$$

where

$$F(z) = \int_{z_o}^{z} \sqrt{f(\xi)}\, d\xi$$

and A and B are constants.

In the following section analysis for the electric field following this line is given while in the next chapters the surface impedance and the solution for the temperature profile are presented.

3.1. Approximate solution for the electric field using the W.K.B. Method - normal incidence

Consider equation (2.17), namely

$$\frac{\partial^2 E(z)}{\partial z^2} + K_o^2(\varepsilon_r' - \sin^2\theta_o)E(z) - j\,\omega\mu\{\sigma(T_a)\exp[\beta \cdot T/(1 + T/T_a)] + \omega\varepsilon_o\varepsilon_r''\}\,E(z) = 0 \qquad (2.17)$$

If we consider the case of normal incidence, then $\sin\theta_o$ equals zero and drops out from equation (2.17)

Rewriting (2.17) for the case of normal incidence in the more convenient form

$$\frac{\partial^2 E(z)}{\partial z^2} + [\alpha - j\eta(T)]\,E(z) = 0 \qquad (3.3)$$

where

$$\alpha = K_o^2\,\varepsilon_r' \qquad (3.4)$$

$$\eta(T) = \omega\mu\{\sigma(T_a)\exp[\beta \cdot T/(1 + T/T_a)] + \omega\varepsilon_o\varepsilon_r''\} \qquad (3.5)$$

We note that since the function $\eta(T)$ is a very slowly varying function of z, the W.K.B. approximate solution for (3.5) is readily shown to be [Appendix B]

$$E(z) = [f(T)]^{-\frac{1}{4}}\left[A\exp\left(-j\int\sqrt{f(T)}\,dz\right) + B\exp\left(j\int\sqrt{f(T)}\,dz\right)\right] \qquad (3.6)$$

where

$$f(T) = \alpha - j\eta(T) \qquad (3.7)$$

It is simple to show that

$$f^{\frac{1}{2}}(T) = \pm\frac{1}{\sqrt{2}}\left[\left(\sqrt{\alpha^2 + \eta^2(T)} + \alpha\right)^{\frac{1}{2}} - j\left(\sqrt{\alpha^2 + \eta^2(T)} - \alpha\right)^{\frac{1}{2}}\right] \qquad (3.8)$$

where either sign in (3.8) is acceptable since they both yield the same expression when (3.8) is substituted in (3.6).

In order to evaluate the multiplier in (3.6) we simplify (3.8) in the form

$$f^{\frac{1}{2}}(T) = \gamma(T) - j\,\lambda(T) \tag{3.9}$$

where

$$\gamma(T) = \frac{1}{\sqrt{2}}\left[\sqrt{\alpha^2 + \eta^2(T)} + \alpha\right]^{\frac{1}{2}} \tag{3.10}$$

$$\lambda(T) = \frac{1}{\sqrt{2}}\left[\sqrt{\alpha^2 + \eta^2(T)} - \alpha\right]^{\frac{1}{2}} \tag{3.11}$$

the function $f^{\frac{1}{4}}(T)$ hence becomes

$$f^{\frac{1}{4}}(T) = \left(\frac{+}{+}j\right)\left\{\left(\frac{\sqrt{\gamma^2(T) + \lambda^2(T)} + \gamma(T)}{2}\right)^{\frac{1}{2}} - j\left(\frac{\sqrt{\gamma^2(T) + \lambda^2(T)} - \gamma(T)}{2}\right)^{\frac{1}{2}}\right\} \tag{3.12}$$

which can be further simplified by introducing ψ defined by

$$\psi = \arctan - \left(\frac{\sqrt{\gamma^2(T) + \lambda^2(T)} - \gamma(T)}{\sqrt{\gamma^2(T) + \lambda^2(T)} + \gamma(T)}\right)^{\frac{1}{2}} \tag{3.13}$$

Hence

$$f^{\frac{1}{4}}(T) = \left[\gamma^2(T) + \lambda^2(T)\right]^{\frac{1}{4}} \exp[j\theta(T)] \tag{3.14}$$

where

$$\theta(T) = \psi(T),\quad \psi(T) + \pi,\quad \psi(T) + \pi/4 \quad \text{and} \quad \psi(T) + 5\pi/4$$

Finally it is simple to show that (3.14) reduces to the form

$$f^{\frac{1}{4}}(T) = \left[\alpha^2 + \eta^2(T)\right]^{1/8} \exp[j\theta(T)] \tag{3.15}$$

Therefore equation (3.6) becomes

$$E(z) = \exp[-j\theta(T)] \cdot \{A \exp(-j \int_0^z \gamma \, dz - \int_0^z \lambda \, dz) + B \exp(j \int_0^z \gamma \, dz + \int_0^z \lambda \, dz)\}/[\alpha^2 + \eta^2(T)]^{1/8} \tag{3.16}$$

Letting

$$m(z) = \int_0^z \gamma \, dz, \quad m' = m(h) = \int_0^h \gamma \, dz$$

$$n(z) = \int_0^z \lambda \, dz, \quad n' = n(h) = \int_0^h \lambda \, dz \tag{3.17}$$

we obtain

$$E(z) = \exp[-j\theta(T)] \cdot \{A \exp[-n(z) - jm(z)] + B \exp[n(z) + jm(z)]\}/[\alpha^2 + \eta^2(T)]^{1/8} \tag{3.18}$$

Next we apply the boundary condition given by (2.30) at $z = h$. This leads to

$$0 = A \exp(-n' - jm') + B \exp(n' + jm')$$

hence

$$B = - A \exp(-2n' - 2jm')$$

Substituting again in equation (3.18), we obtain

$$E(z) = A \exp[-n(z) - jm(z) - j\theta(T)] \cdot \{1 - \exp[2(n(z) - n') + 2j(m(z) - m')]\}/(\alpha^2 + \eta^2(T))^{1/8} \tag{3.19}$$

or alternatively

$$E(z) = \frac{A \exp[-n(z)]}{[\alpha^2 + \eta^2(T)]^{1/8}} \{[1 - \cos 2(m(z) - m') \cdot \exp 2(n(z) - n')]^2$$

$$+ [\sin 2(m(z) - m') \cdot \exp 2(n(z) - n')]^2\}^{\frac{1}{2}}$$

$$\cdot \exp\{-j\theta(T) - j\, m(z) + j\, \xi(z)\} \qquad (3.20)$$

where

$$\xi(z) = \arctan \{-\frac{\sin 2(m(z) - m') \cdot \exp 2(n(z) - n')}{1 - \cos(m(z) - m') \cdot \exp 2(n(z) - n')}\} \qquad (3.21)$$

Equation (3.20) is the solution for the electric field at any point inside the slab given explicitly in terms of the temperature. By doing so, we have decoupled the pair of the differential equations (2.17) and (2.28), hence allowing simultaneous solution of equations (3.20) and (2.26) for T and E(z). Some typical numerical results based on this procedure are presented in the next section.

3.1.1. *Numerical examples*

In order to illustrate the electric field profile inside the slab for different test frequencies and incident fields we choose $\omega = 10^{10}$ rad./sec., $\omega = 10^{11}$ rad./sec. and $\omega = 10^{12}$ rad./sec. and two values of the incident field are considered, merely 1000 volt/m and 500 V/m. The results are limited to the semiconductor state with activation energy $\Delta E = 0.3$ ev. After transition the material turns to a metal with a temperature independent conductivity [10], although in some special cases it is reported that the polyconductor film is still in the semiconductor state but with different activation energy equals to 0.09 ev. [14]. In all cases the work involves only the semiconductor state before transition where $\Delta E = 0.3$ ev. The other parameters are assigned the following constant values:

$T_a = 300\ ^\circ K$ $\qquad$ $h = 1$ cm

$\sigma(300) = 10^{-1}$ Mho. cm^{-1} $\qquad$ $S = 10$ cm

$\Delta E = 0.3$ e.v.

$\varepsilon_r' = 10$ $\qquad$ $k_a = 5 \times 10^{-2}$ W. cm^{-1} . $^\circ K^{-1}$

$\varepsilon_r'' = 0.001$

$K_S = 11/57.79$ $\quad W \cdot cm^{-1} \cdot {}^\circ K^{-1}$

$\varepsilon = 0.6$

$\delta = 1.37 \times 4.18 \times 10^{-8}$ $\quad Watt/m^2$

where the physical parameters from ΔE to δ are typical [4,18]. The results are presented graphically in Figures (3.1) to (3.6)

3.2. Surface impedance

The surface impedance is the factor that governs the relation between the electric and magnetic fields at the boundary of the medium in question as given previously by equation (2.3). Since by virtue of (2.4)

$$Z_S(E_o) = - E_y/H_x\Big|_{z=0}$$

hence the electric and magnetic fields at the surface $z = 0$ must be evaluated in order to evaluate $Z_S(E_o)$.

Using equations (3.15) and (3.19) the electric field at any point z can be expressed as

$$E(z) = A \cdot f^{-\frac{1}{4}}(T) \cdot \{\exp[-n(z) - jm(z)] - \exp[n(z) - 2n') + j(m(z) - 2m')]\} \qquad (3.22)$$

which at $z = 0$ becomes

$$E(0) = A \cdot f^{-\frac{1}{4}}(T_S) \cdot \{1 - \exp[-2(n' + jm')\} \tag{3.23}$$

Differentiating (3.22) with respect to z and evaluating at $z = 0$, we obtain

$$\left.\frac{dE}{dz}\right|_{z=0} = -\frac{1}{4} f^{-5/4}(T_S) \cdot \left.\frac{df(T)}{dz}\right|_{z=0} \cdot A\{1 - \exp[-2(n' + jm')]\}$$

$$-f^{-\frac{1}{4}}(T_S) \cdot A \cdot [\lambda(T_S) + j\gamma(T_S)] \cdot \{1 + \exp[-2(n' + jm')]\} \tag{3.24}$$

where the following relations have been used to arrive at (3.24):

$$n(0) = 0$$

$$m(0) = 0$$

$$\frac{d}{dz} n(z) = \frac{d}{dz} \int_0^z \lambda(T)\, dz = \lambda(T)$$

and

$$\frac{d}{dz} m(z) = \frac{d}{dz} \int_0^z \gamma(T)\, dz = \gamma(T)$$

Since the surface impedance is given by the expression (see equations (2.4) and (2.6))

$$Z_S(E_o) = -E_y / \frac{1}{j\omega\mu} \frac{dE_y}{dz}$$

$$= -j\omega\mu\, E(0) / \left.\frac{dE(z)}{dz}\right|_{z=0} \tag{3.25}$$

we proceed to substitute equations (3.23) and (3.24) in (3.25) to obtain

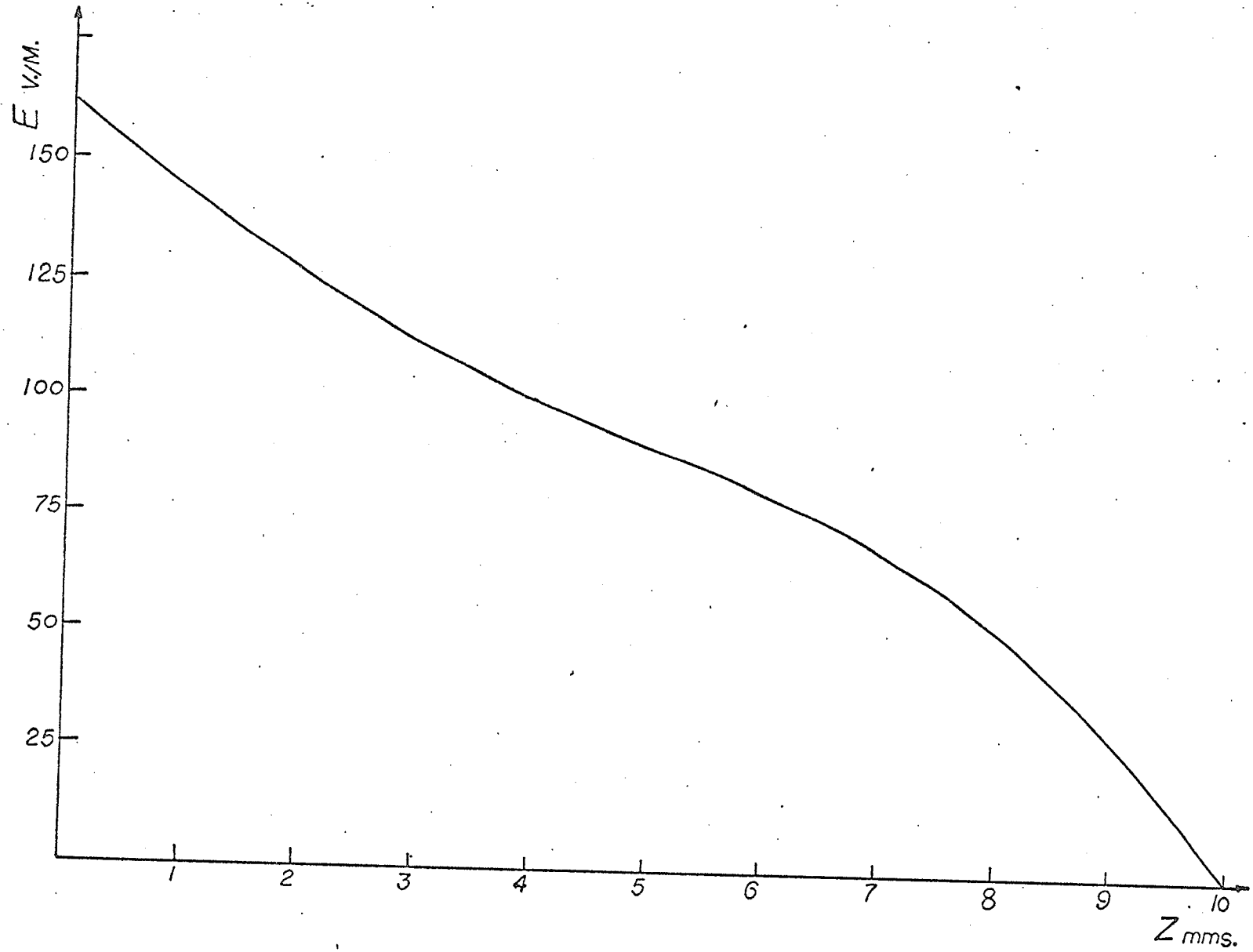

Fig. 3.1 Transmitted electric field versus distance inside the slab for E^i = 1000 V•/m• and $\omega = 10^{10}$ rad./sec..

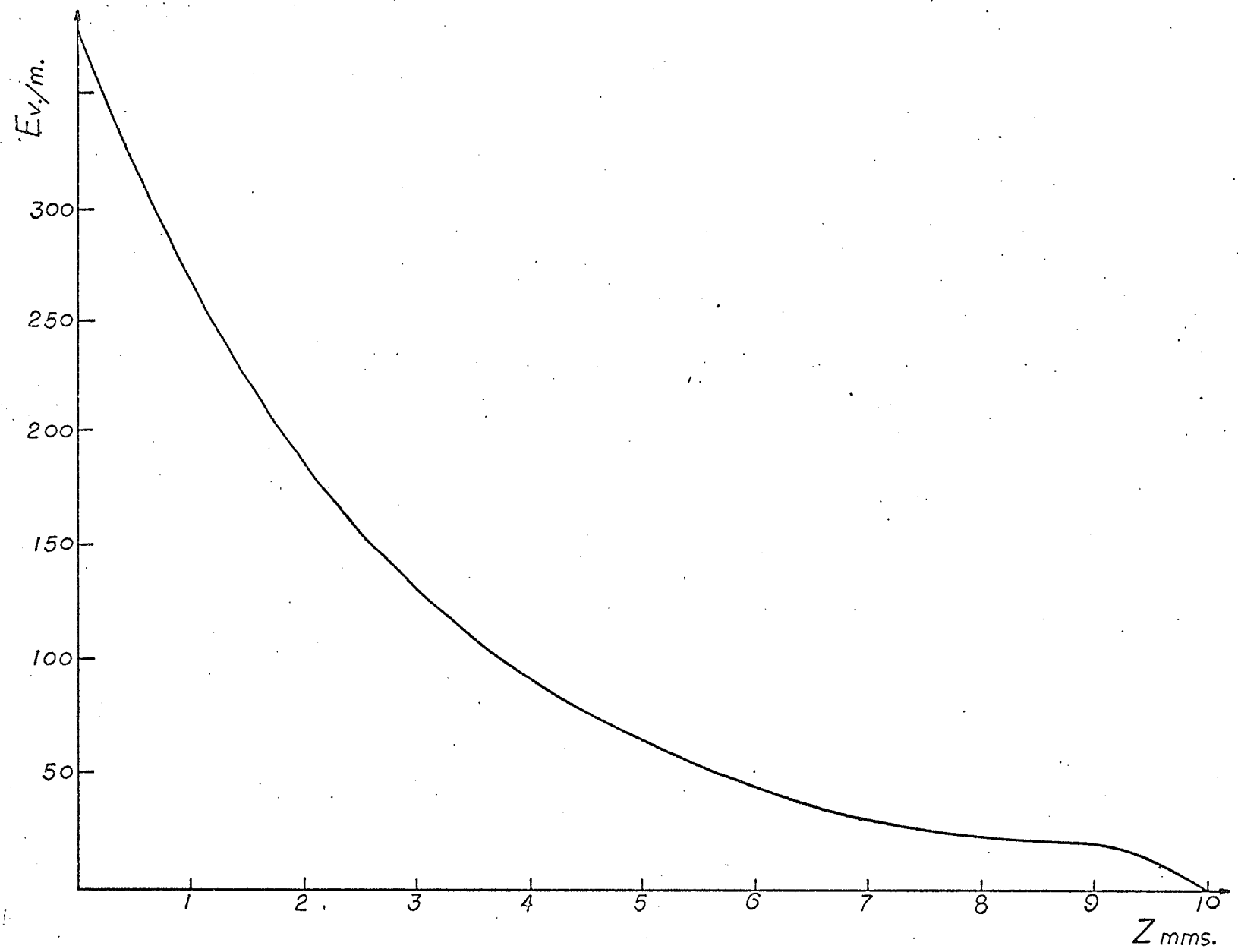

Fig. 3.2 Transmitted electric field versus distance inside the slab for E^i = 1000 V·/m· and $\omega = 10^{11}$ rad./sec.

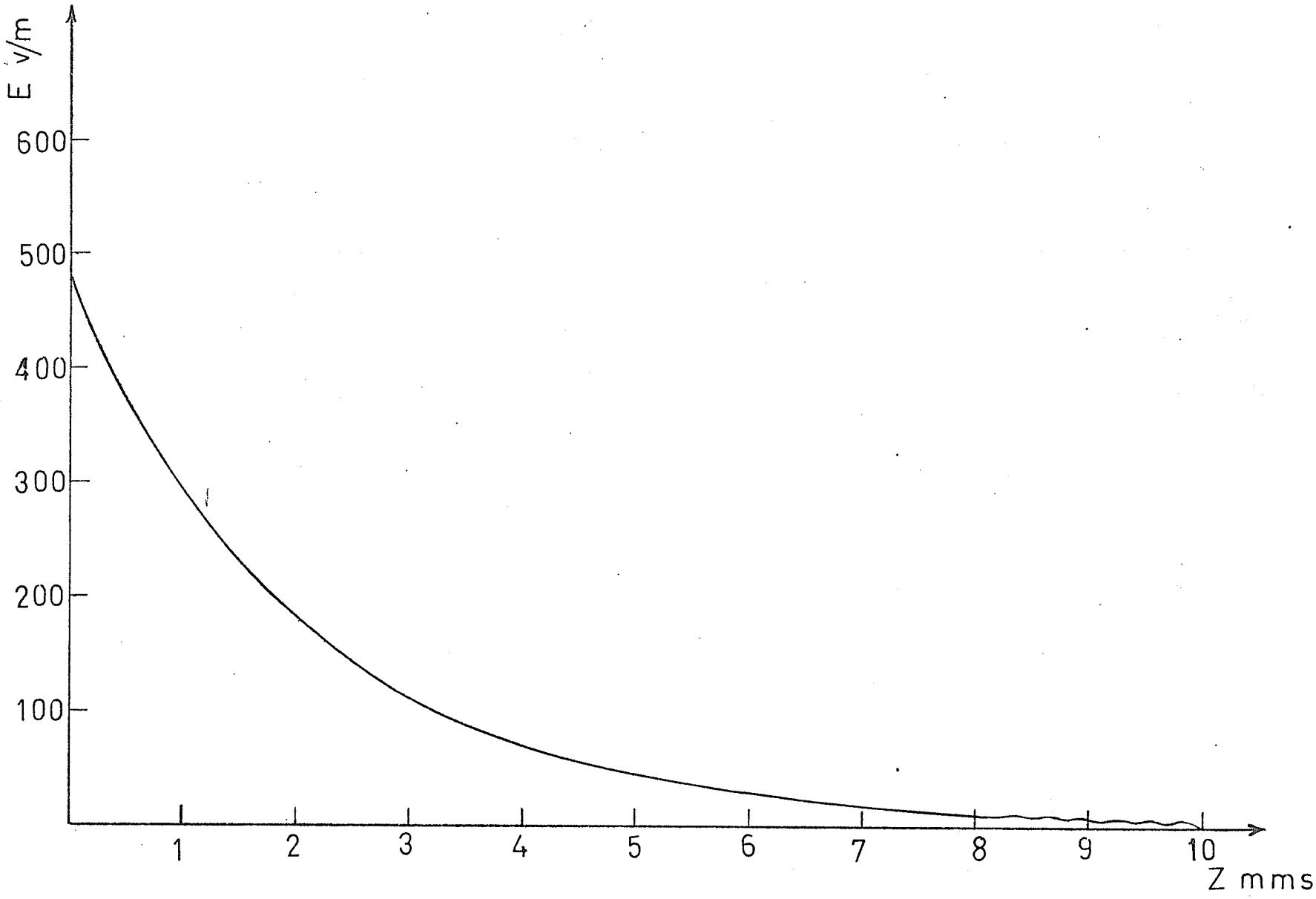

Fig. 3.3 Transmitted electric field versus distance inside the slab for E^i = 10000 V•/m• and $\omega = 10^{12}$ rad./sec.

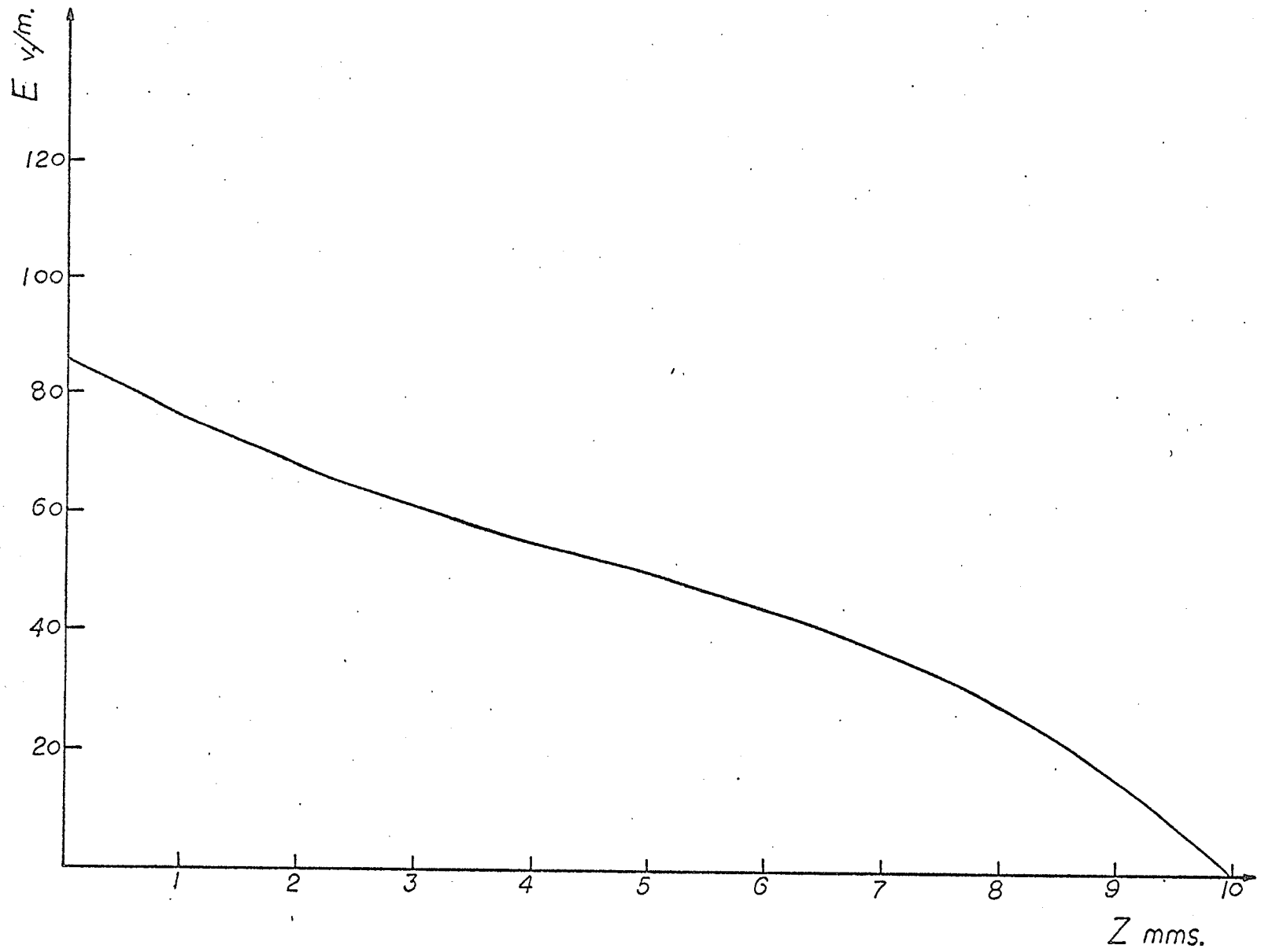

Fig. 3.4 Transmitted electric field versus distance inside the slab for E^i = 500 V•/m• and $\omega = 10^{10}$ rad./sec.

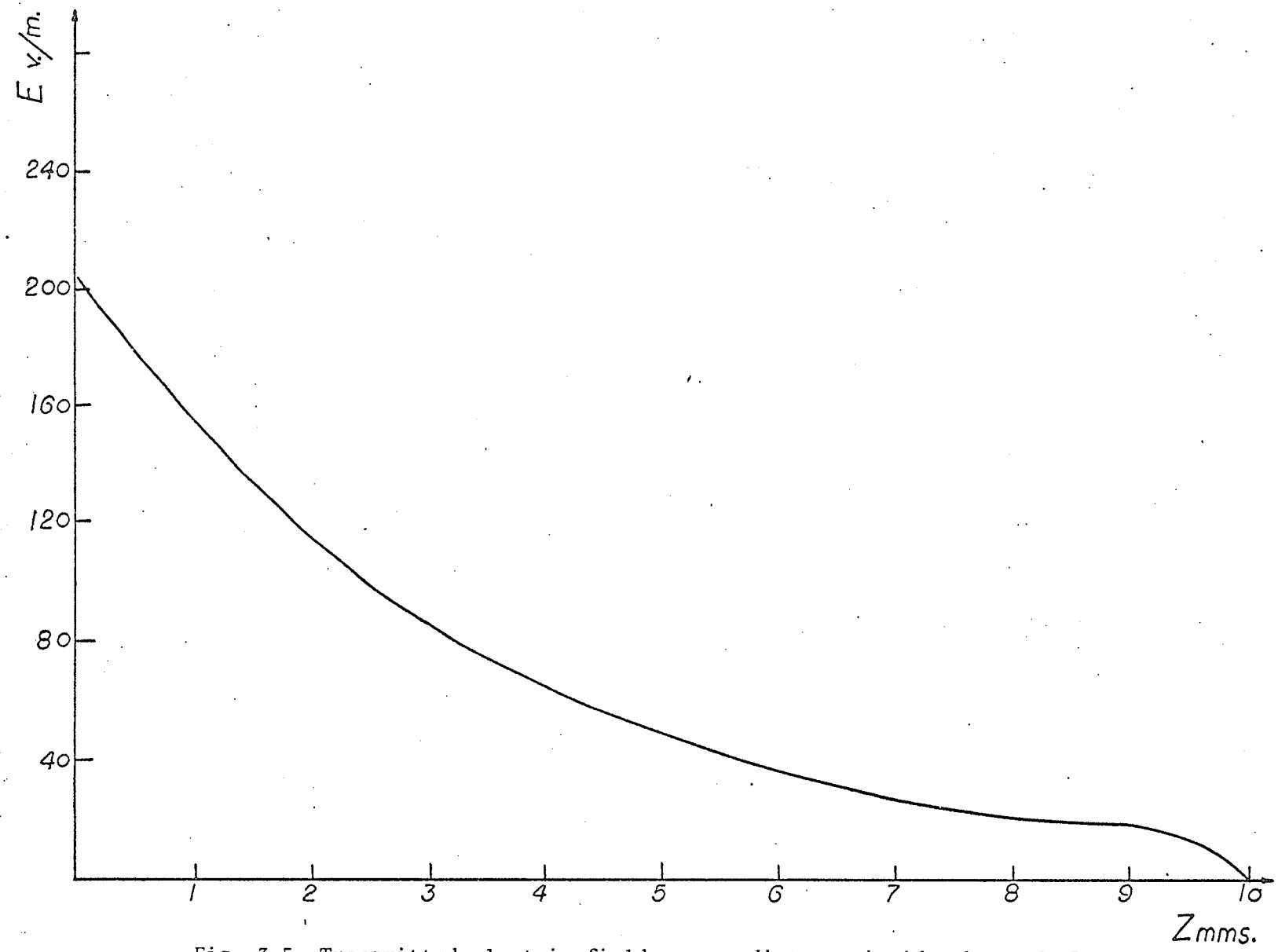

Fig. 3.5 Transmitted electric field versus distance inside the slab for $E^i = 500$ V•/m• and $\omega = 10^{11}$ rad./sec.

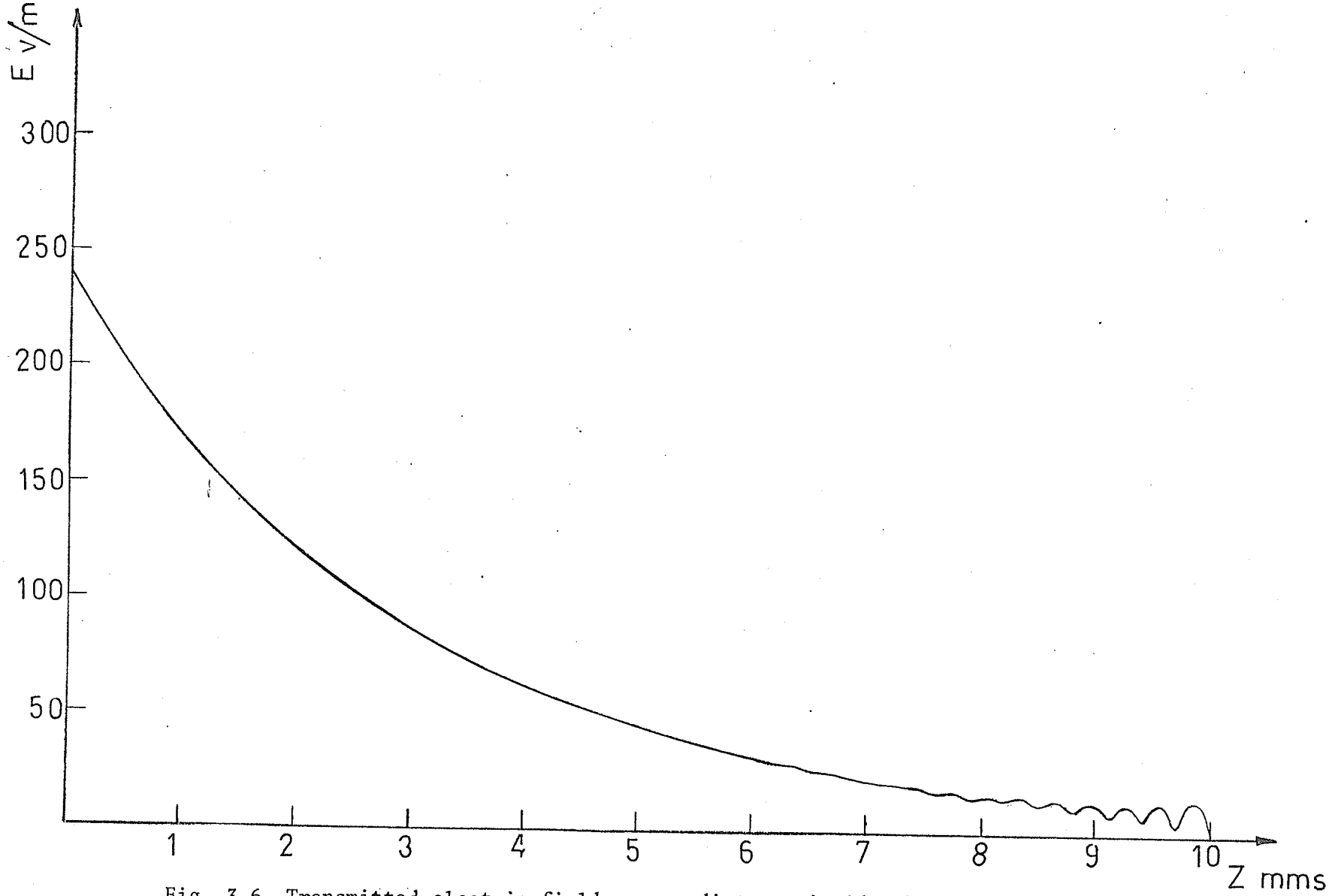

Fig. 3.6 Transmitted electric field versus distance inside the slab for E^i = 500 V•/m• and $\omega = 10^{12}$ rad./sec.

$$Z_S(E_o) = j\omega\mu f^{-\frac{1}{4}}(T_S) \cdot \{1 - \exp[-2(n' + jm')]\}/\{\frac{1}{4} f^{-5/4}(T_S) \cdot$$

$$\left.\frac{df(T)}{dz}\right|_{z=0} \cdot [1 - \exp\{-2(n' + jm')\}] + f^{-\frac{1}{4}}(T_S) \cdot$$

$$(\lambda(T_S) + j\gamma(T_S)) \cdot [1 + \exp\{-2(n' + jm')\}]\} \qquad (3.26)$$

or alternatively

$$Y_S(E_o) = \frac{df(T)/dz|_{z=0}}{j\omega\mu \cdot 4f(T_S)} + \{\frac{\lambda(T_S) + j\gamma(T_S)}{j\omega\mu}\}$$

$$\cdot \frac{\exp(n' + jm') + \exp(-n' - jm')}{\exp(n' + jm') - \exp(-n' - jm')}$$

where $Y_S(E_o) = 1/Z_S(E_o)$. Since

$$\coth x = [\exp(x) + \exp(-x)]/[\exp(x) - \exp(-x)]$$

therefore

$$Y_S(E_o) = \frac{df(T)/dz|_{z=0}}{j\omega\mu \cdot 4f(T_S)} + \frac{\lambda(T_S) + j\gamma(T_S)}{j\omega\mu} \cdot \coth(n' + jm') \qquad (3.27)$$

To evaluate $\left.\frac{df(T)}{dz}\right|_{z=0}$ we have from equation (3.7)

$$f(T) = \alpha - j\eta(T)$$

which leads to

$$\frac{df(T)}{dz} = - j \frac{d\eta(T)}{dz}$$

$$= - j \frac{d\eta(T)}{dT} \cdot \frac{dT}{dz} \qquad (3.28)$$

Differentiating equation (3.5) with respect to T we obtain

$$\frac{d\eta(T)}{dT} = \omega\mu\sigma(T_a) \cdot \frac{\beta}{(1 + T/T_a)^2} \cdot \exp[\beta T/(1 + T/T_a)] \qquad (3.29)$$

at $z = 0$ we have $T = T_S$, so equation (3.28) becomes

$$\frac{df(T)}{dz}\Big|_{z=0} = -j\omega\mu\sigma(T_a) \cdot \frac{\beta}{(1 + T_S/T_a)^2} \cdot \exp[\beta T_s/(1 + T_s/T_a)] \cdot \frac{dT}{dZ}\Big|_{z=0} \qquad (3.30)$$

Since from (2.32) we have

$$\frac{dT}{dz}\Big|_{z=0} = 4\delta\ \varepsilon T_a^3\ T_S/k_a \qquad (3.31)$$

then upon substitution, equation (3.30) becomes

$$\frac{df(T)}{dz}\Big|_{z=0} = -j\omega\mu\sigma(T_a)\ \frac{\beta}{(1 + T_S/T_a)^2} \cdot \exp[\beta \cdot T_S/(1 + T_S/T_a)] \cdot 4\delta\varepsilon\ T_a^3\ T_S/k_a \qquad (3.32)$$

where

$$\frac{dT}{dz}\Big|_{z=0} = -\frac{dT}{dn}\Big|_{z=0}$$

Since $\hat{z}$ and $\hat{n}$ are in opposite directions.

Equation (3.32) together with (3.27) leads to the final expression for $Z_S(E_o)$:

$$Z_S(E_o) = \frac{-\sigma(T_a) \cdot \beta}{4f(T_S) \cdot (1 + T_S/T_a)^2} \cdot \exp[\beta T_s/(1 + T_s/T_a)] \cdot \frac{4\delta\varepsilon T_a^3\ T_s}{k_a} + \frac{\lambda(T_S) + j\gamma(T_S)}{j\omega\mu} \coth(n' + jm') \qquad (3.33)$$

It is seen that the real and imaginary parts of the surface impedance are functions of the surface temperature, which is in turn a

function of the incident field.

3.2.1. *Numerical examples*

To illustrate the variation of the effective surface impedance with the incident field three test frequencies are chosen, these are $\omega = 10^{10}$ rad./sec., $\omega = 10^{11}$ rad./sec., and $\omega = 10^{12}$ rad./sec.. The results are shown in Figs. (3.7) to (3.9). All other parameters are assigned the values given in section (3.1.1). It should be emphasized that other curves displaying such variations as $Z_S(E_o)$ with T_S . . . etc. can be also obtained by referring to the original equations if necessary or combining graphs already presented.

3.3. Temperature distribution

Consider equation (2.26) which governs the temperature distribution within the slab, namely

$$k_a \frac{d^2T}{dz^2} + [\sigma(T_a) \cdot \exp\{\beta T/(1 + T/T_a)\} + \omega\varepsilon_o\varepsilon_r''] \cdot |E(z)|^2 = 0 \qquad (2.26)$$

where, by virtue of equation (3.20), $|E(z)|$ is given by

$$|E(z)| = \frac{A \cdot \exp[-n(z)]}{[\alpha^2 + \eta^2(T)]^{1/8}} \{[1 - \cos 2(m(z) - m') \cdot \exp 2(n(z) - n')]^2 + [\sin 2(m(z) - m') \cdot \exp 2(n(z) - n')]^2\}^{\frac{1}{2}} \qquad (3.34)$$

In order to derive an approximate solution for (2.26), a numerical procedure is employed. Since we are dealing with a boundary-value problem, in which the boundary conditions are specified at more than one point within the z range of the function, the finite difference

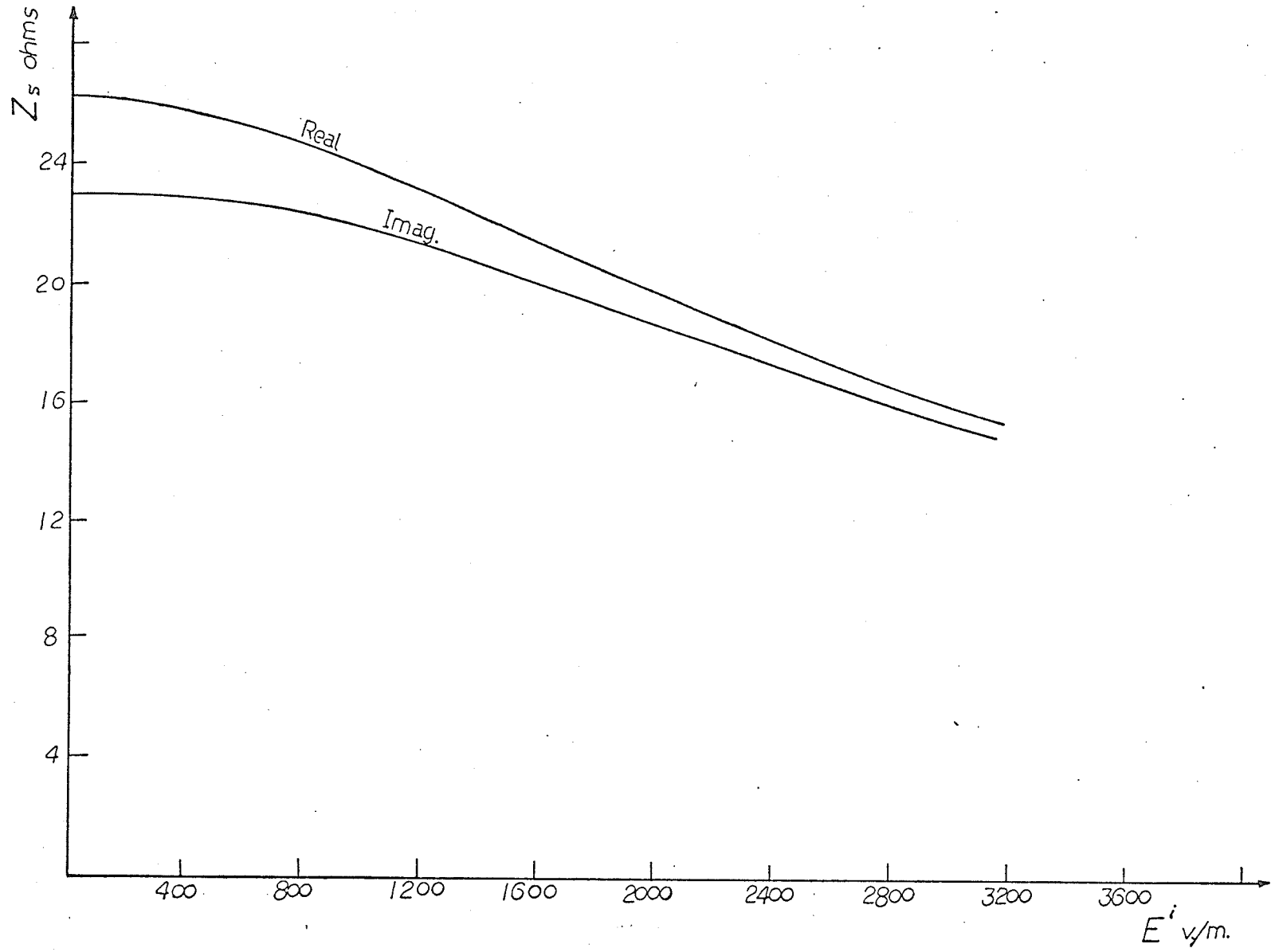

Fig. 3.7 Surface impedance versus incident field for $\omega = 10^{10}$ rad./sec.

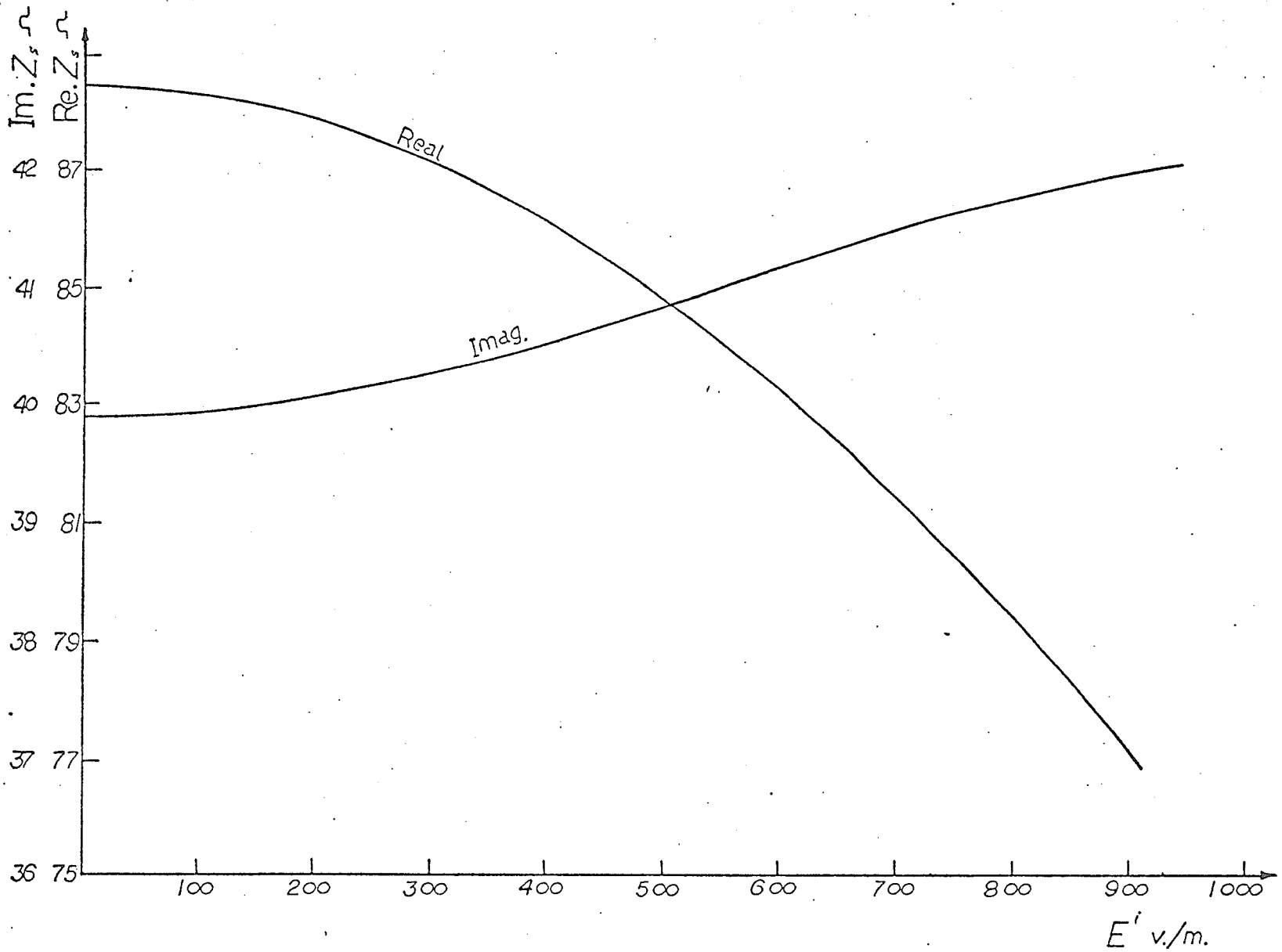

Surface impedance versus incident field for $\omega = 10^{11}$ rad./sec.

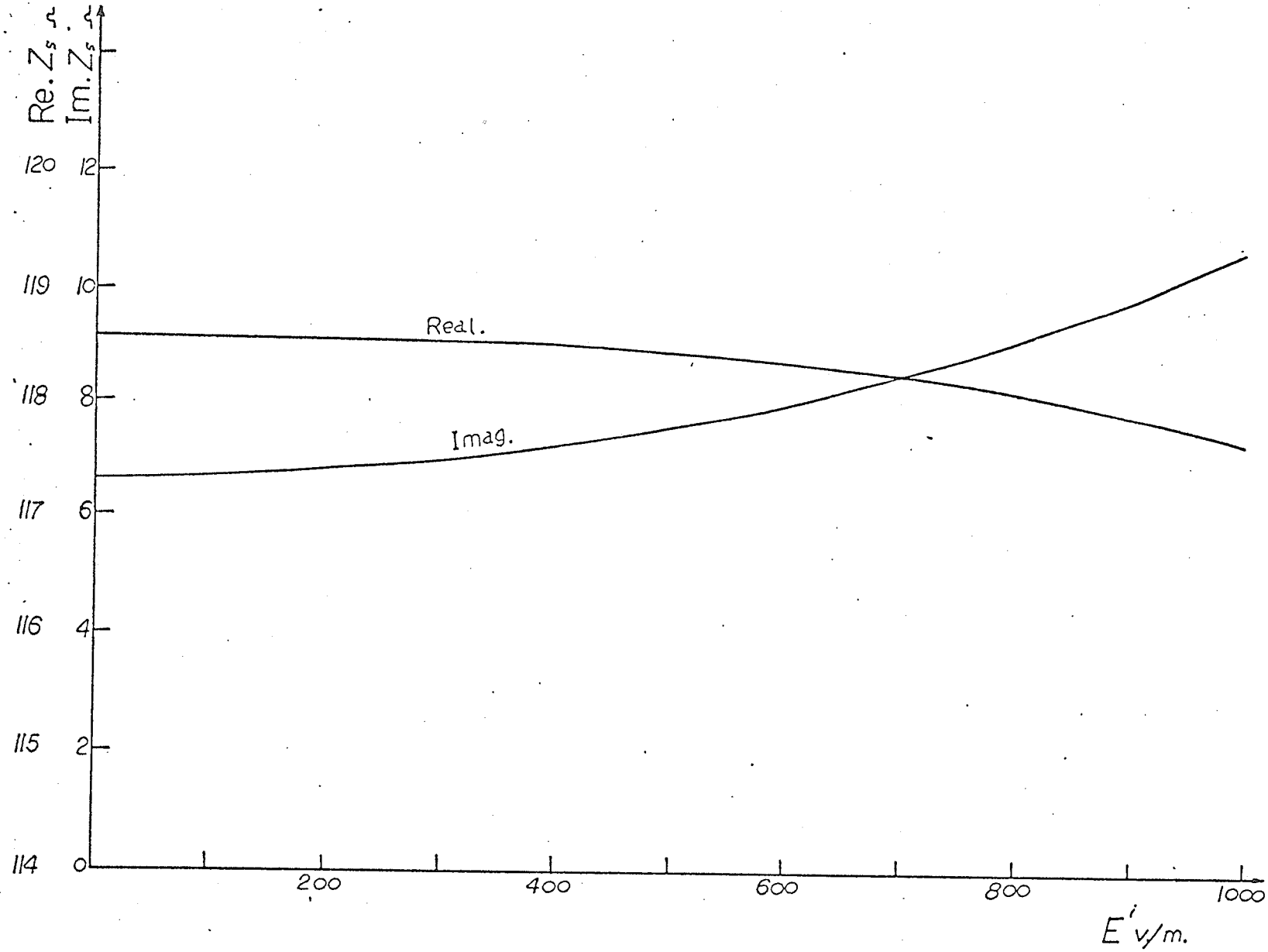

Fig. 3.9 Surface impedance versus incident field for $\omega = 10^{12}$ rad./sec.

method is the most convenient method to use from the point of view of computational time. A description of the numerical procedure is given in some detail in Appendix C. Numerical results are presented in the following section.

3.3.1. *Numerical Results*

Figs. (3.10) through (3.15) present curves showing the variation of the temperature as well as the conductivity throughout the slab for the three test frequencies $\omega = 10^{10}$ rad./sec., $\omega = 10^{11}$ rad./sec., and $\omega = 10^{12}$ rad./sec.. Also two values of incident fields are considered as shown in figures. All other parameters mentioned previously in section (3.1.1) are kept constant and assigned the same values as before.

A discussion regarding the method used and the accuracy obtained is given in Appendix C.

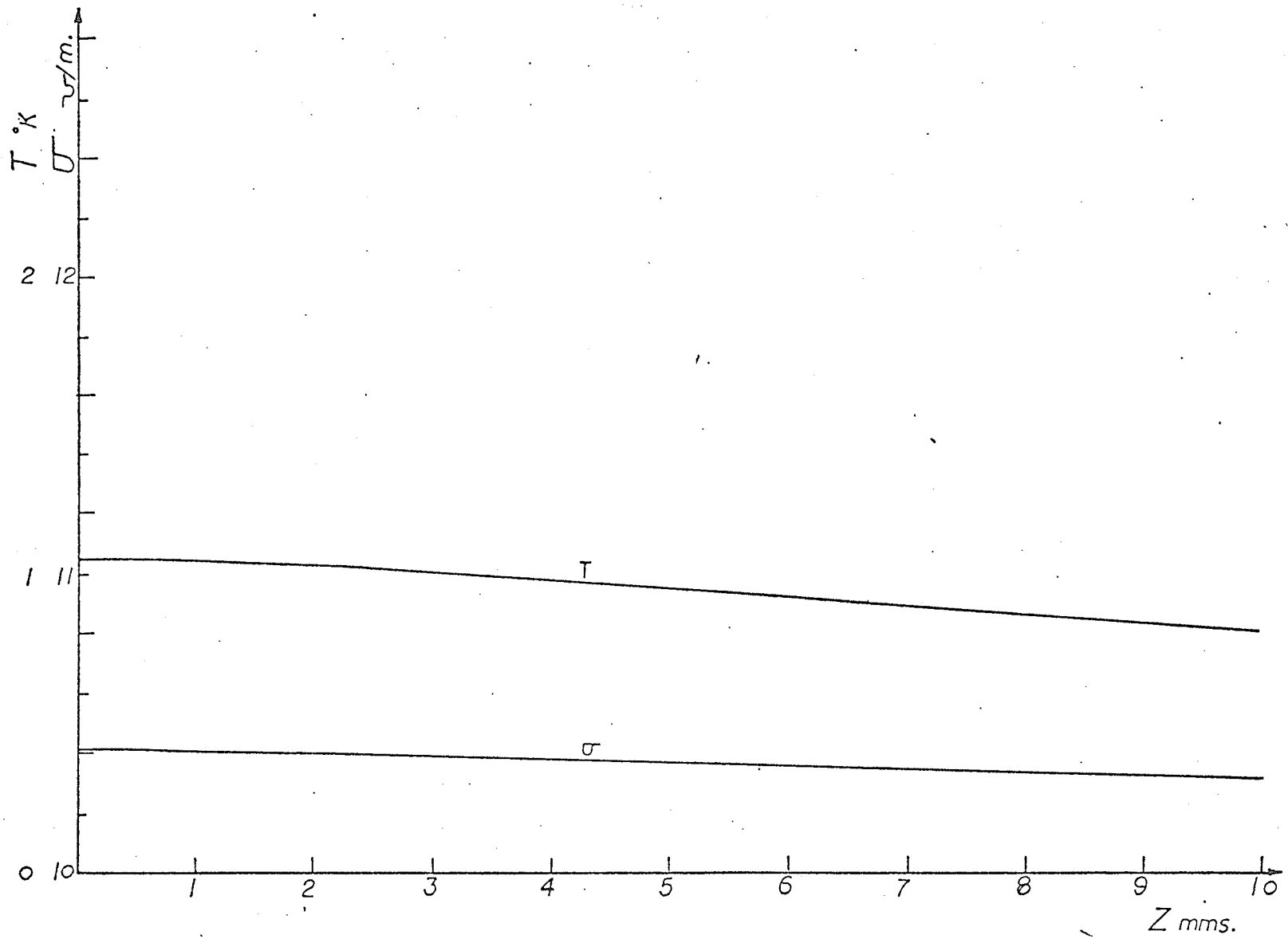

Fig. 3.10 Conductivity and temperature (above 300°K) versus distance inside the slab for E^i = 500 V•/m• and $\omega = 10^{10}$ rad./sec.

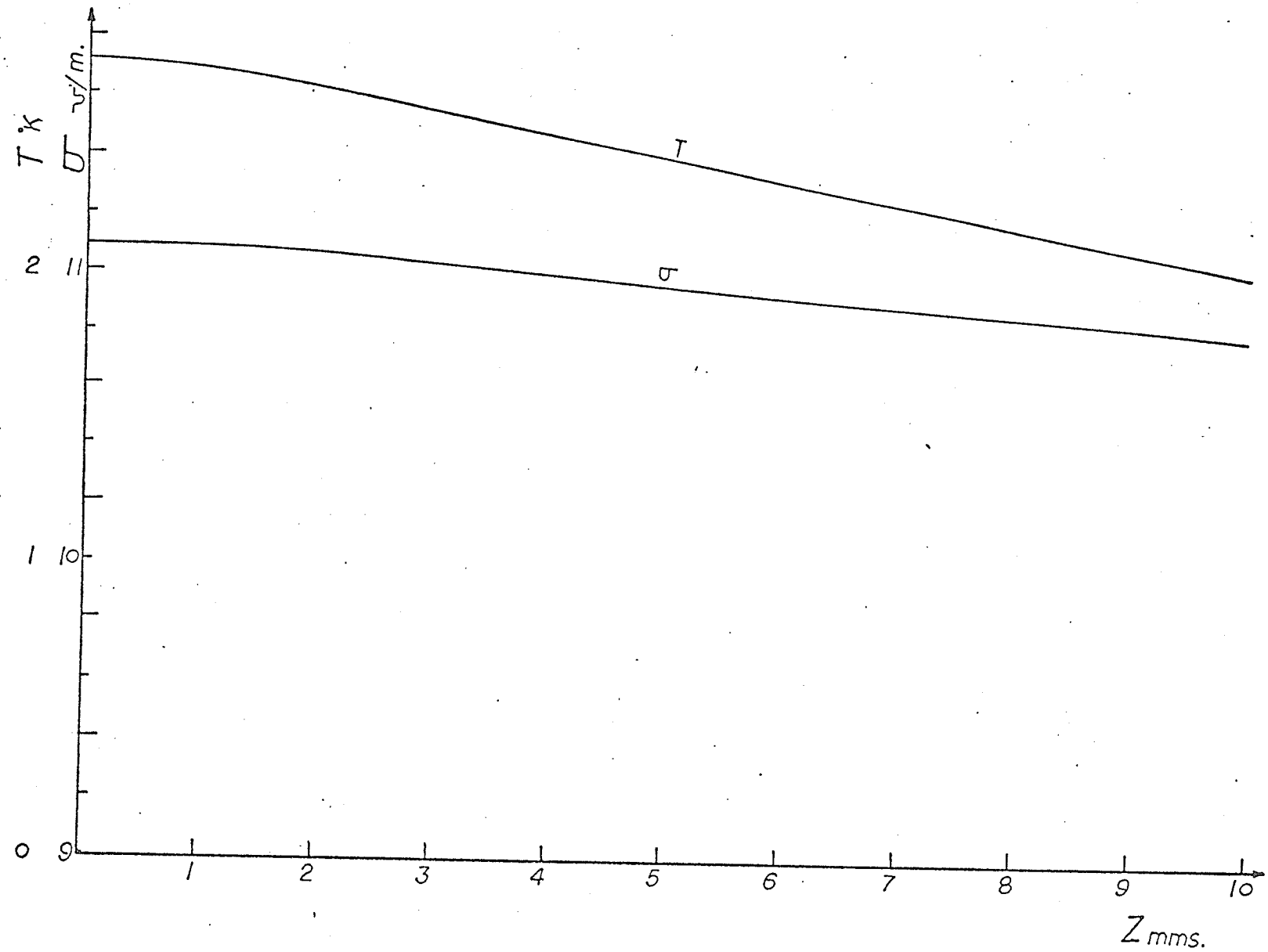

Fig. 3.11 Conductivity and temperature (above 300°K) versus distance inside the slab for E^i = 500 V/m and $\omega = 10^{11}$ rad./sec.

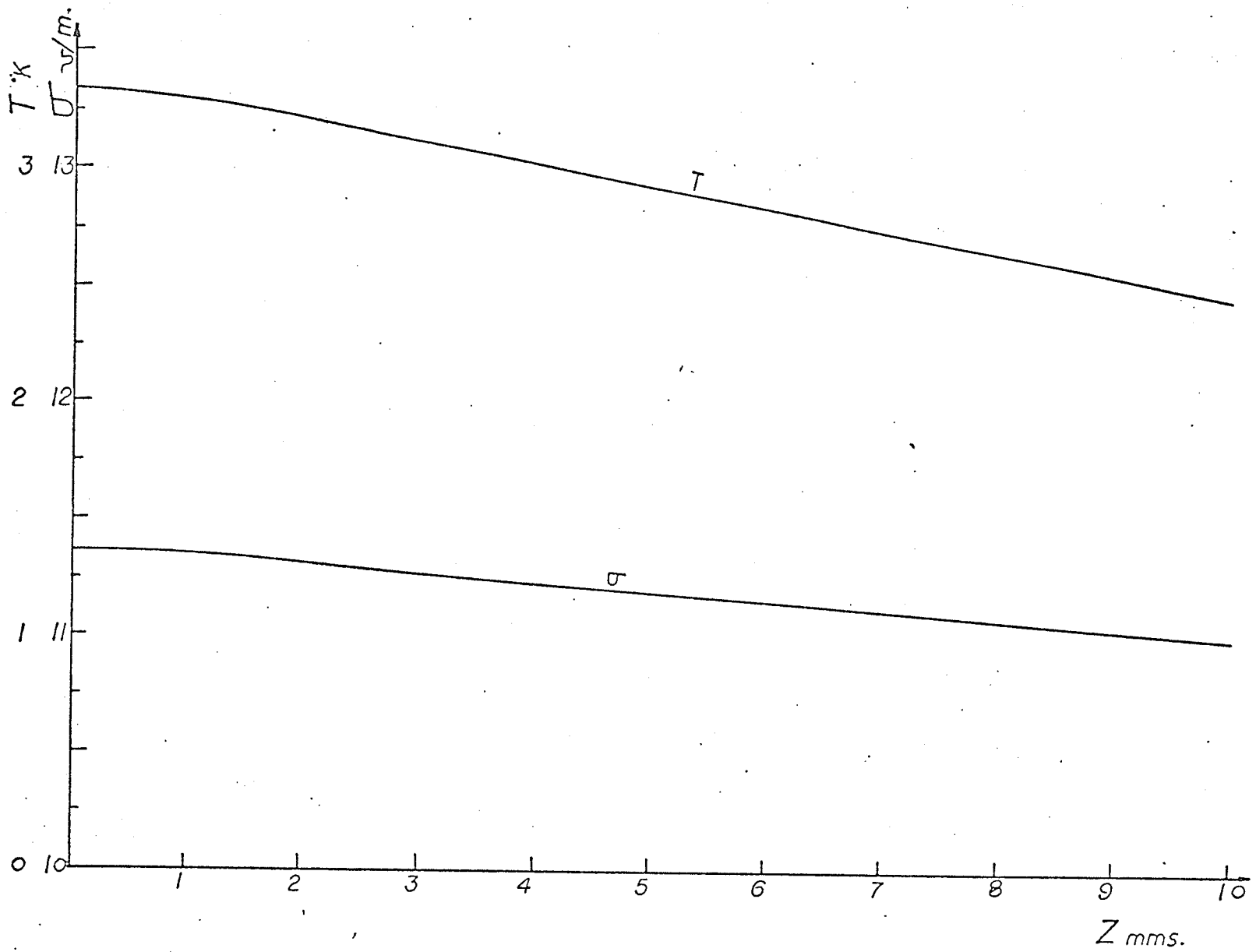

Fig. 3.12 Conductivity and temperature (above 300°K) versus distance inside the slab for E^i = 500 V·/m· and $\omega = 10^{12}$ rad./sec.

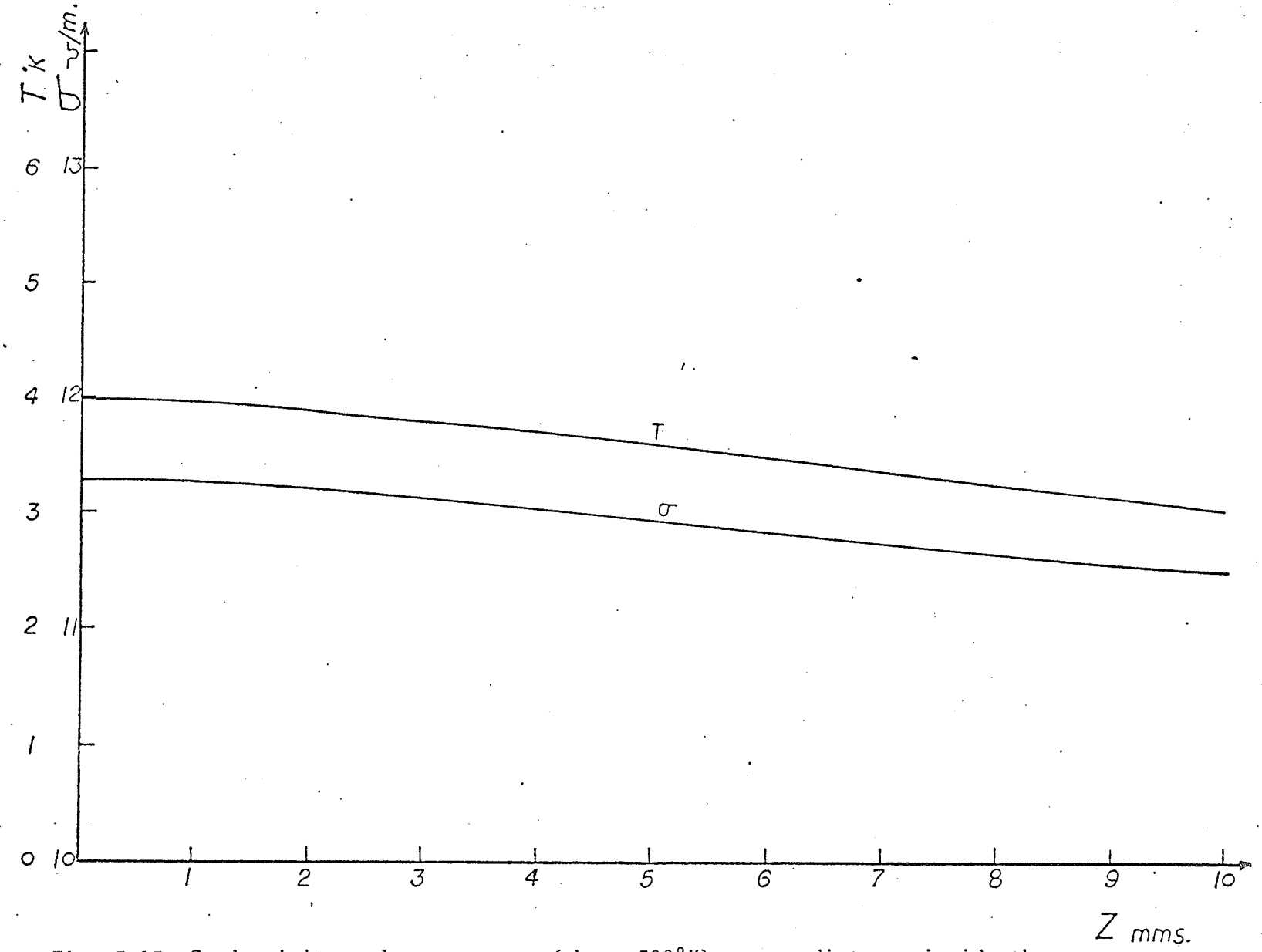

Fig. 3.13 Conductivity and temperature (above 300°K) versus distance inside the slab for E^i = 1000 V•/m• and $\omega = 10^{10}$ rad./sec.

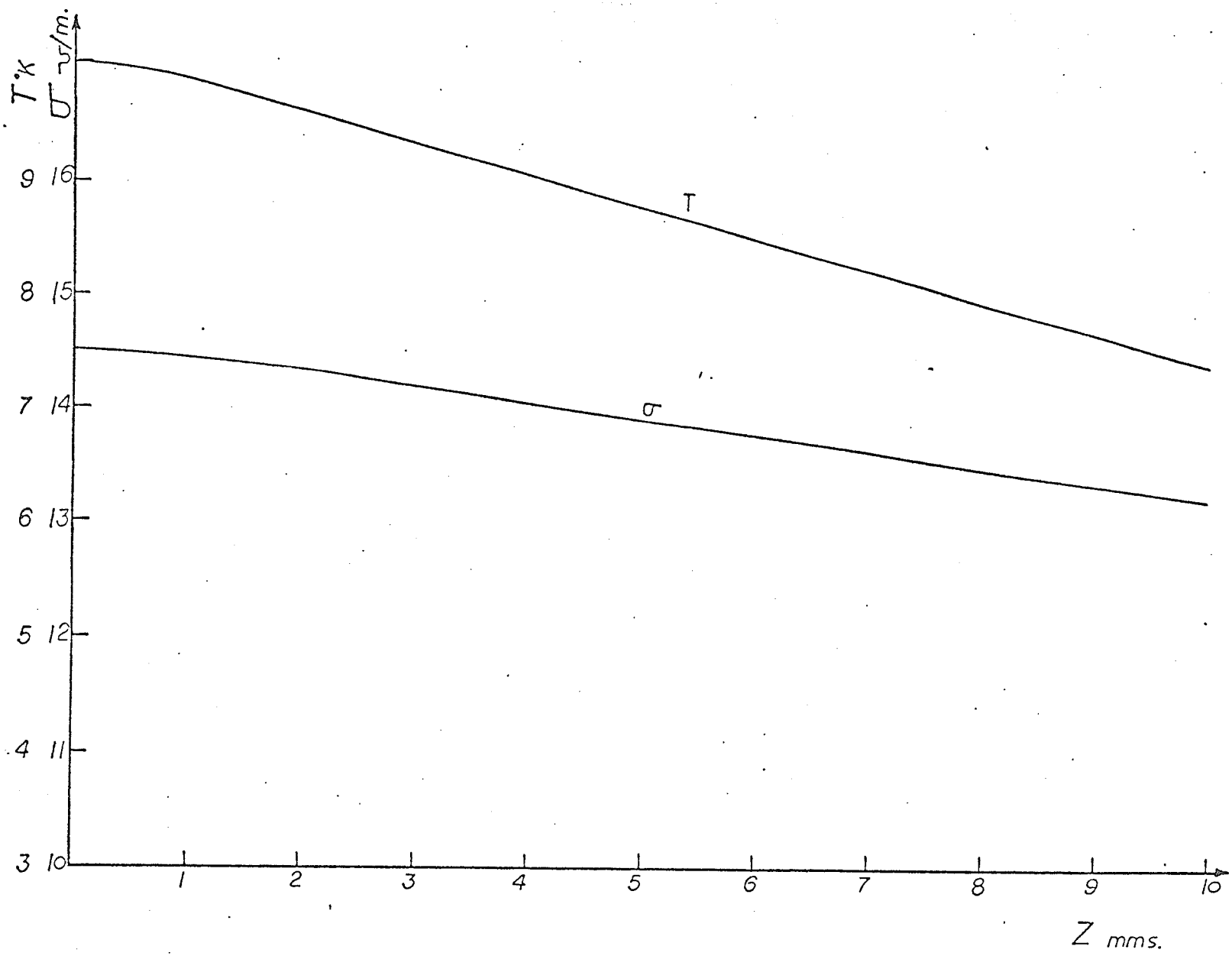

Fig. 3.14 Conductivity and temperature (above 300°K) versus distance inside the slab for E^i = 1000 V·/m· and $\omega = 10^{11}$ rad./sec.

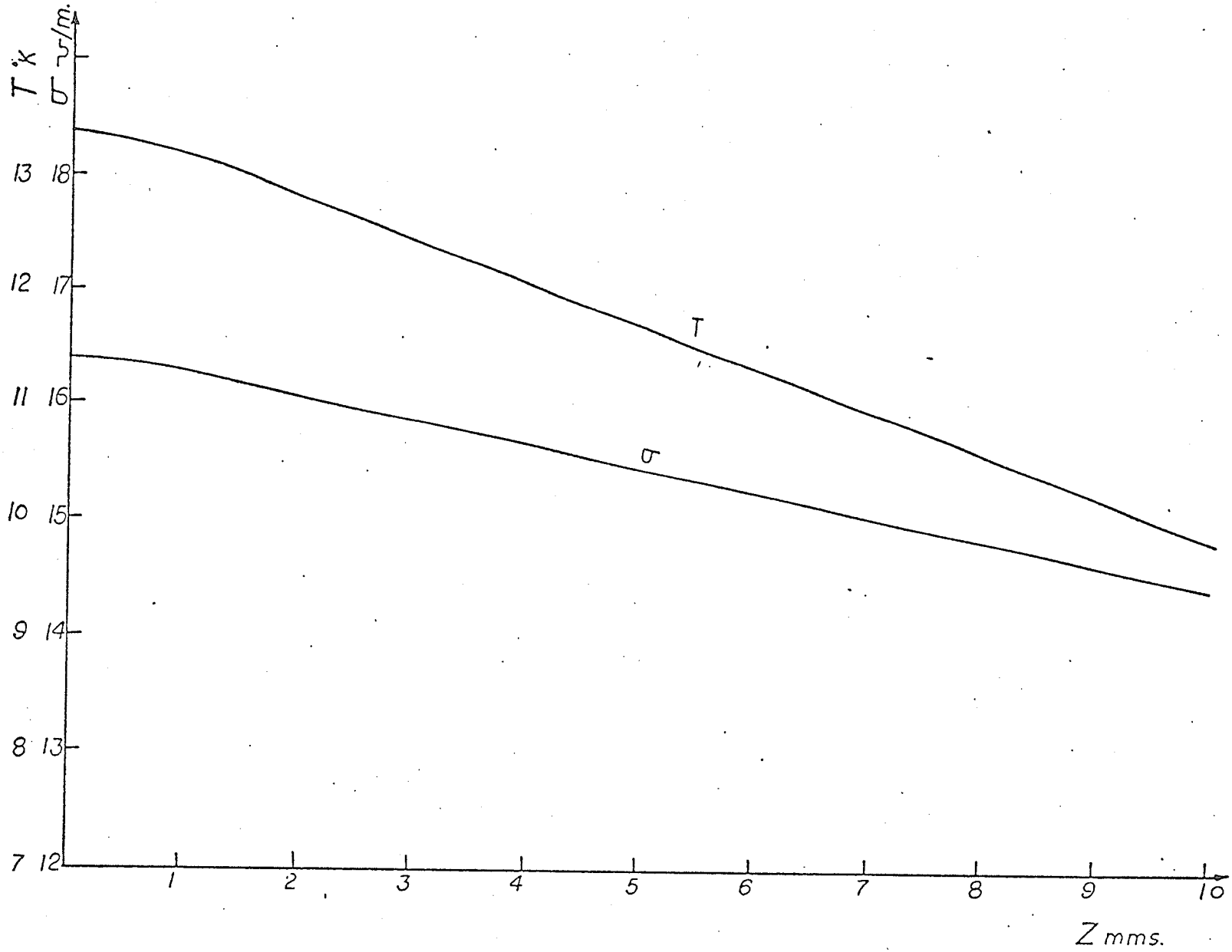

Fig. 3.15 Conductivity and temperature (above 300°K) versus distance inside the slab for E^i = 1000 V•/m• and $\omega = 10^{12}$ rad./sec.

4. DISCUSSION

Because of the nonlinear interaction between the electrical and thermal parameters selected to a polyconductor slab irradiated by microwave power, the mathematical analysis of the problem is reduced to the solution of two coupled second order ordinary differential equations. Since no closed form solution has been found, these equations are solved quasi analytically after physically reasonable assumptions regarding T versus z are introduced to simplify the analysis. In the analytic part, the W.K.B. method was used and its validity is justified in Appendix B. As for the numerical part, the finite difference method dictatated by the nature of the boundaries encountered and other factors (see section 3.3) has been used. This method has its disadvantages if the system is nonlinear [21] where the generation of the solution may be very difficult. Also the usual computational errors such as the round-off error and the incapability of the computer to retain but finite number of digits adds to the disadvantages of the method. However, in spite of these difficiencies, a stable solution was obtained within only three iterations for each point of the grid. Hence the method leads to a solution which is more accurate than an approximate analytical solution based on an iterative method as discussed in Chapter 1.

As a check on the accuracy of the results, the extreme cases where the slab tends to be a pure dielectric ($\sigma = o$) or a good conductor ($\sigma/\omega\tilde{\varepsilon}_r >> 1$) were tested. The results for E versus Z (shown for the case of $\sigma = o$ in F.2 p.84) and for the reflection coefficient R are in both cases in complete agreement with the well known solution given in Appendix F.

In the lights of the results obtained, it is shown that several

factors such as frequency, dielectric constant, field intensity . . . etc. affect the power absorbed throughout the material. Analyzing the frequency dependence, it is shown that as the frequency increases the field drops more rapidly inside the slab, but the reflection coefficient decreases, hence allowing higher values of the field to be transmitted through the medium [see Figs. (3.1) to (3.6)]. This results in a higher overall power absorbed through the slab as evident from the higher temperature rise above the initial temperature for higher frequencies as shown in Figs. (3.10) to (3.15).

On the other hand, the power absorbed is also dependent on the real part of the relative dielectric constant ε_r'. At lower frequencies the rate of decay of the electric field inside the slab for higher values of ε_r' (up to 70) is considerably less than the corresponding case with smaller ε_r' [see Fig. (4.1)]. This in spite of the lower value of the transmitted field allows higher absorption of power inside the slab. This is clear from Fig. (4.2) where the temperature rise for two different values of ε_r' are presented, and also from Fig. (4.3) where the surface temperatures for several values of ε_r' are plotted. On the contrary, at higher frequencies the absorbed power is noticed to decrease considerably with higher values of ε_r'.

Thus the analysis of the dependence of power absorption on both frequency and ε_r' seems to make it possible to optimize the value of ε_r' of the VO_2 to allow optimum power absorbed, hence temperature rise over a wide frequency band. This suggests a new type of thermal sensor for microwave power measurements. One basic feature of such a thermal sensor is the linear relationship between the power incident and the temperature especially at low and moderate power levels [see Fig. (4.4)].

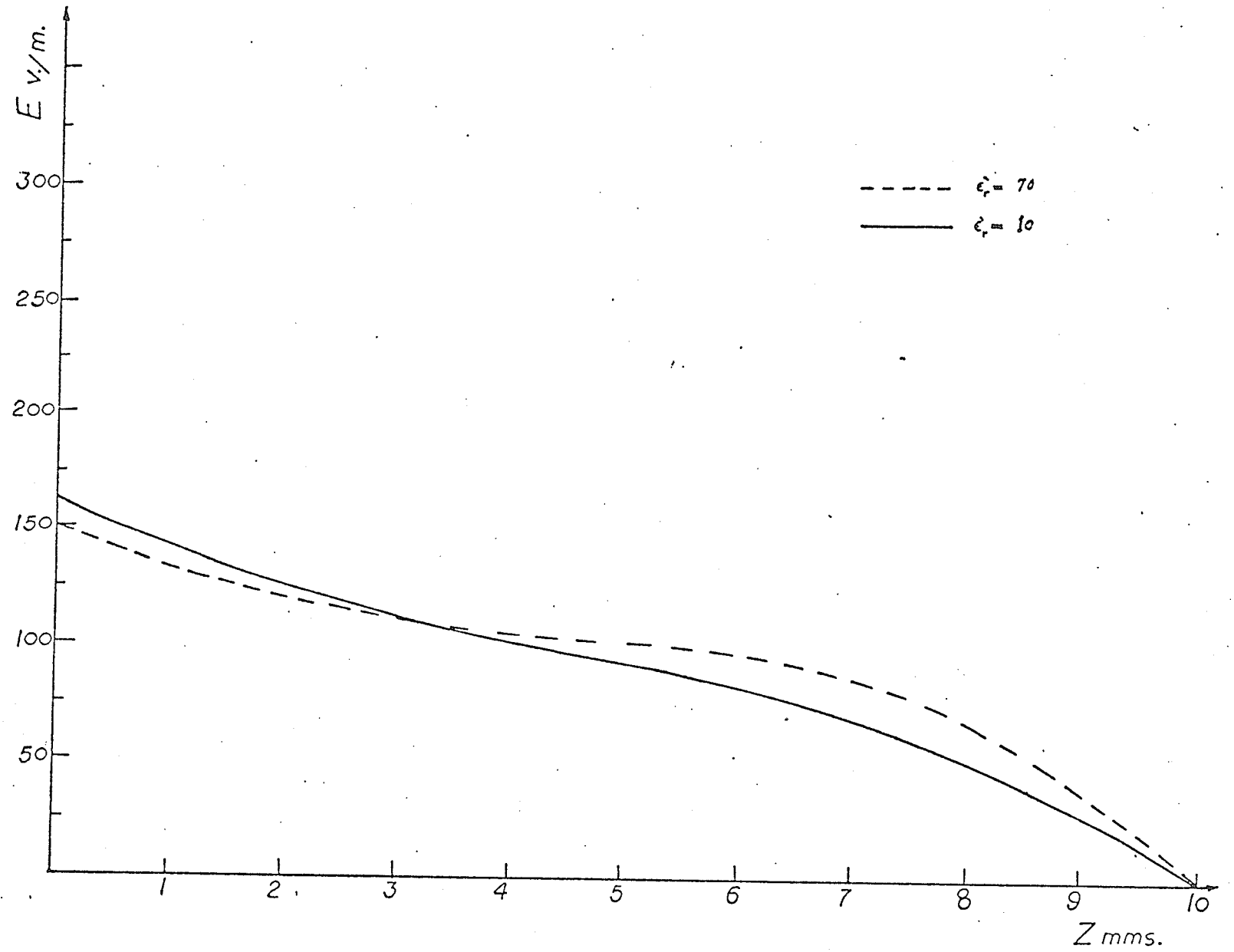

Fig. 4.1 Decay of the transmitted electric field inside the slab with ε_r' as a parameter (E^i = 1000 V·/m· and $\omega = 10^{10}$ rad./sec.)

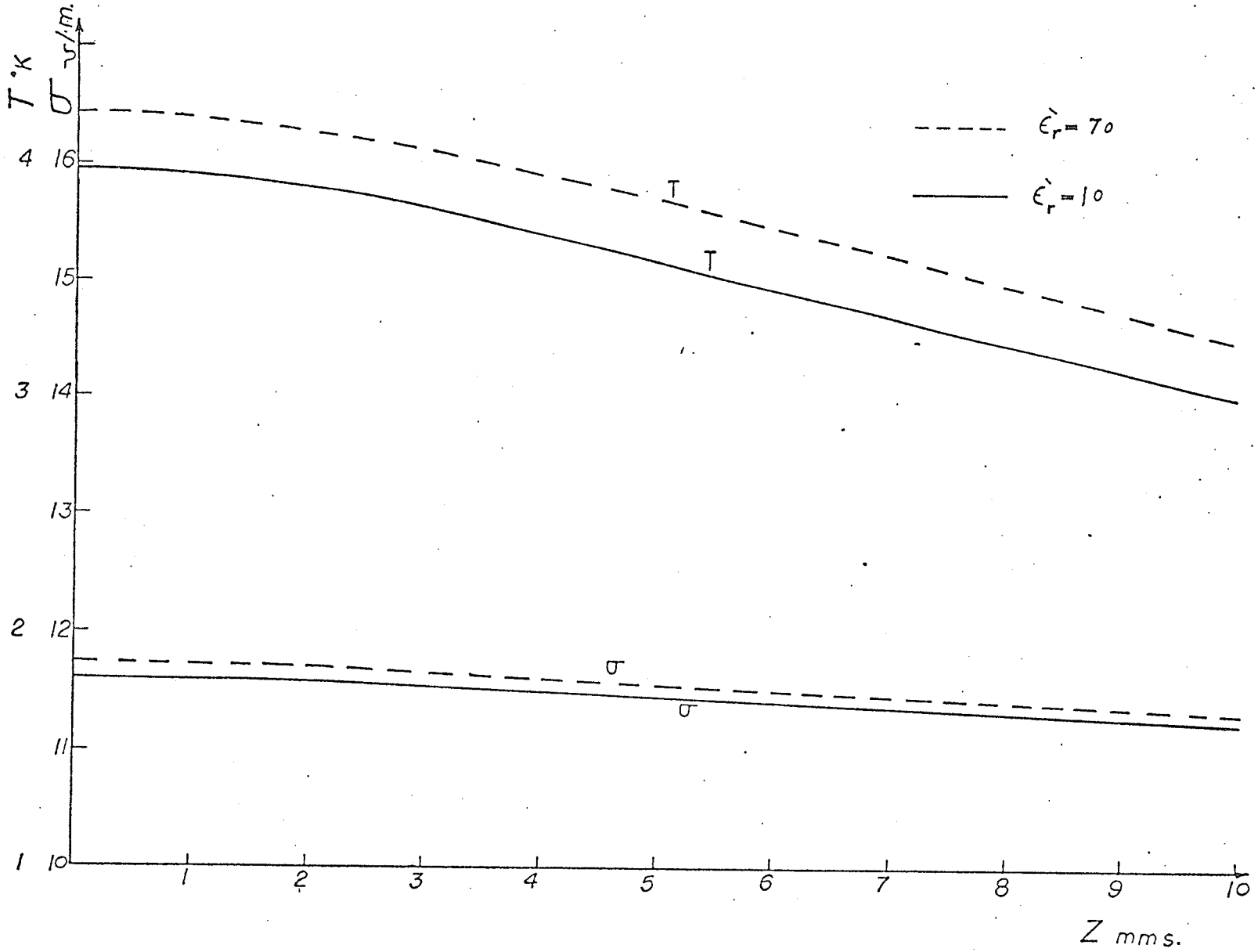

Fig. 4.2 Conductivity and temperature (above 300°K) versus distance inside the slab with ε_r' as a parameter (Ei = 1000.0 V·/m· and $\omega = 10^{10}$ rad./sec.)

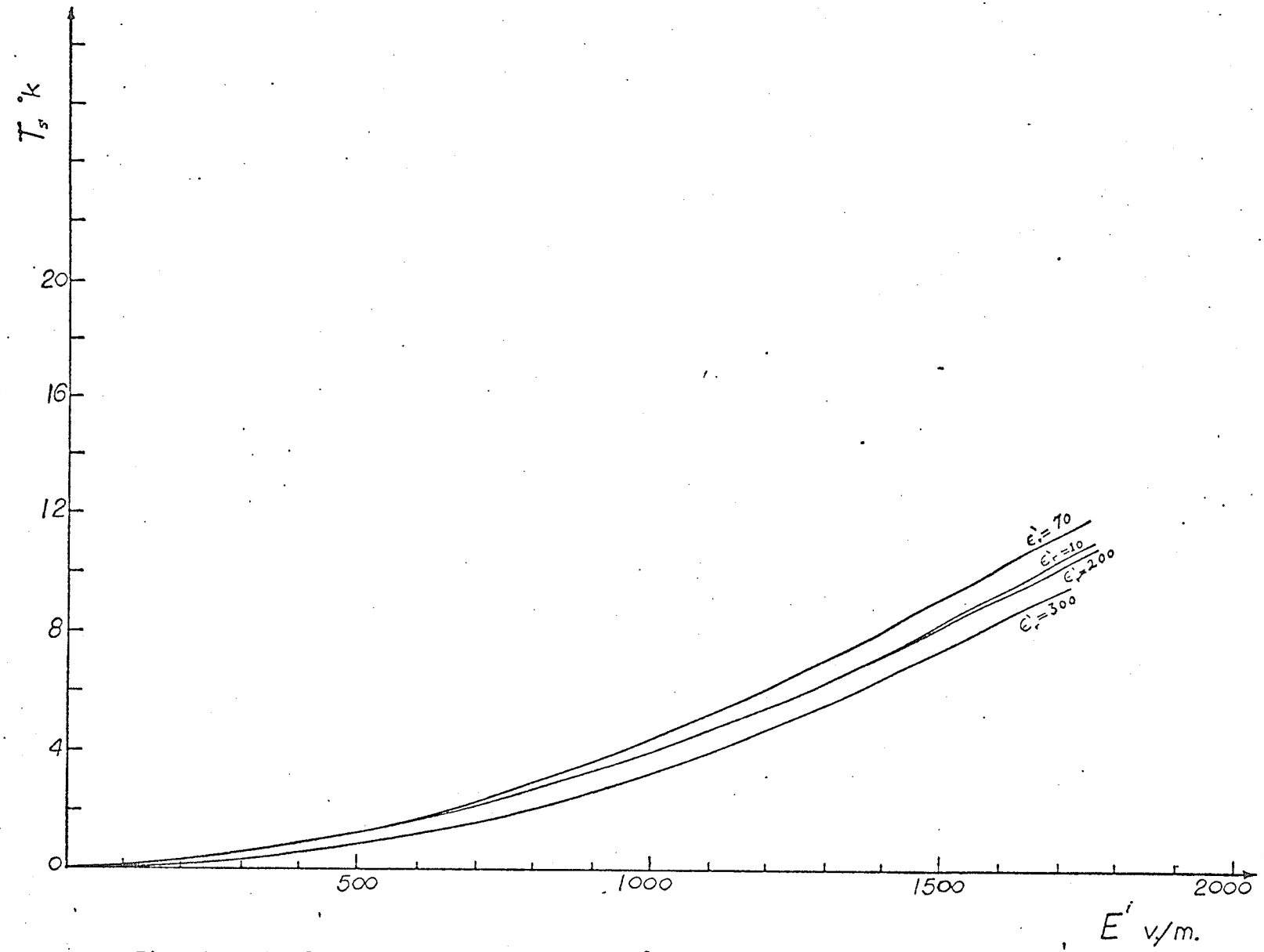

Fig. 4.3 Surface temperature (above 300°K) versus incident field with ε_r' as a parameter ($\omega = 10^{10}$ rad./sec.)

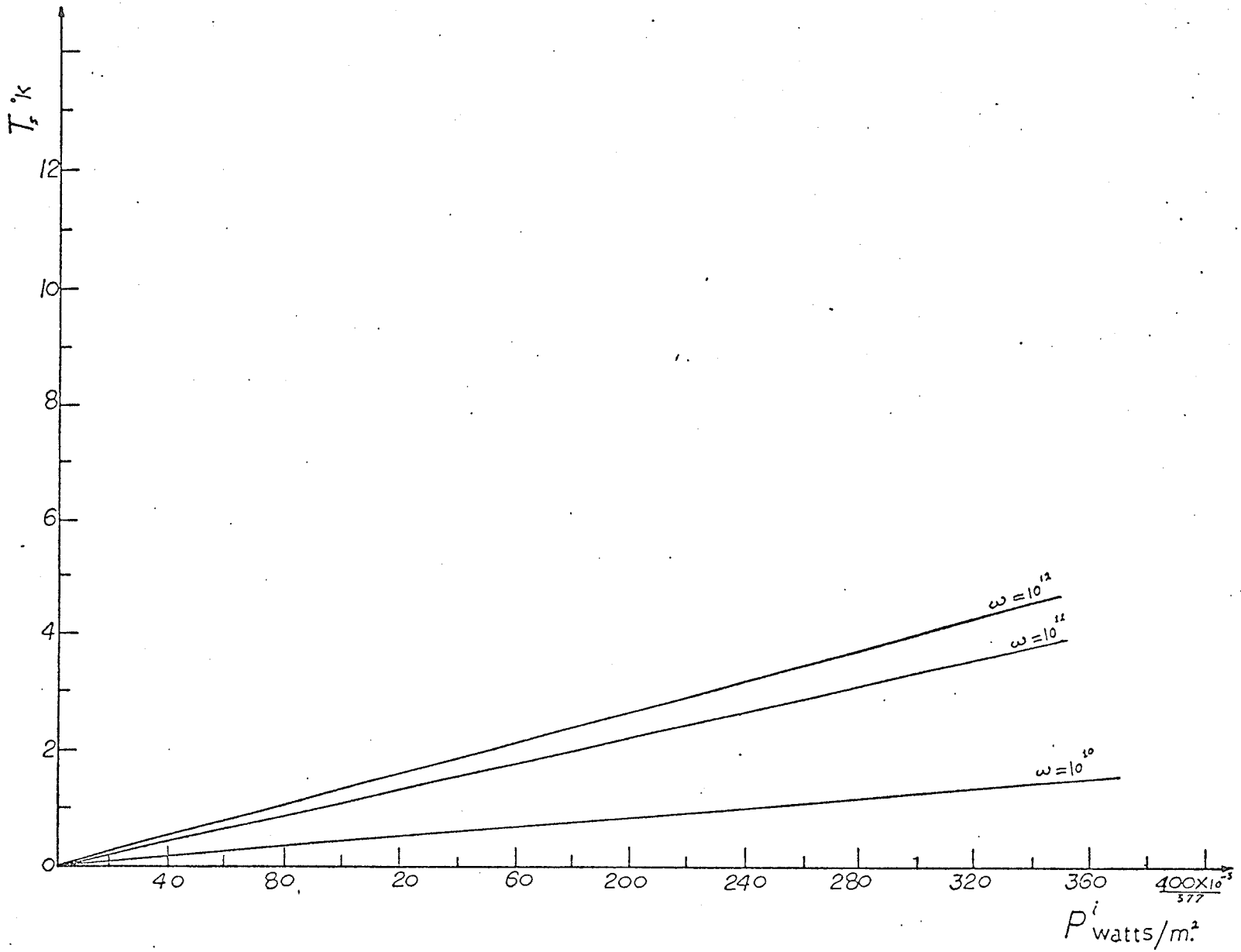

Fig. 4.4 Surface temperature (above 300°K) versus incident power with the frequency as a parameter.

This is of fundamental importance in designing microwave power measuring transducers operating on thermal basis [22]. A detailed discussion of applications proposed for such sensor is given in Chapter 5 and in Appendix D.

In order to increase the power absorbed throughout the slab, an increase in the slope of the conductivity temperature curve is specifically investigated. However, the analysis proves that this leads to a reduction in the absorbed power and the temperature rise, as evident from Figs. (4.5) to (4.7). This could be physically explained as a tendency of the material to behave as a conductor with increasing conductivity resulting in a rapid decay of the field inside it [see Fig. (4.8)] and hence smaller absorptivity of the incident microwave energy. Similar behaviour is also noticed when the imaginary part of the dielectric constant is increased. This, in addition to the fact that a higher conductivity or ε_r'' is necessary for higher power dissipation indicates the presence of a countereffect which limits the power absorbed throughout the material. Thus one of our basic objectives to use the VO_2 slab as a microwave power density sensor can not be achieved unless some means are found for storing significant energy while the material is in the semiconductor state. One way of achieving this is to use a very thin VO_2 film on a substrate of higher thermal capacity. An alternative approach is to dope the polyconductor with an appropriate dielectric material where significant additional energy would be absorbed by and stored in the dielectric such as to affect a large change in the conductivity and hence change the state of the polyconductor. A similar problem was encountered in microwave power drying of oil-based printing ink for the printing industry and was solved by doping the ink with

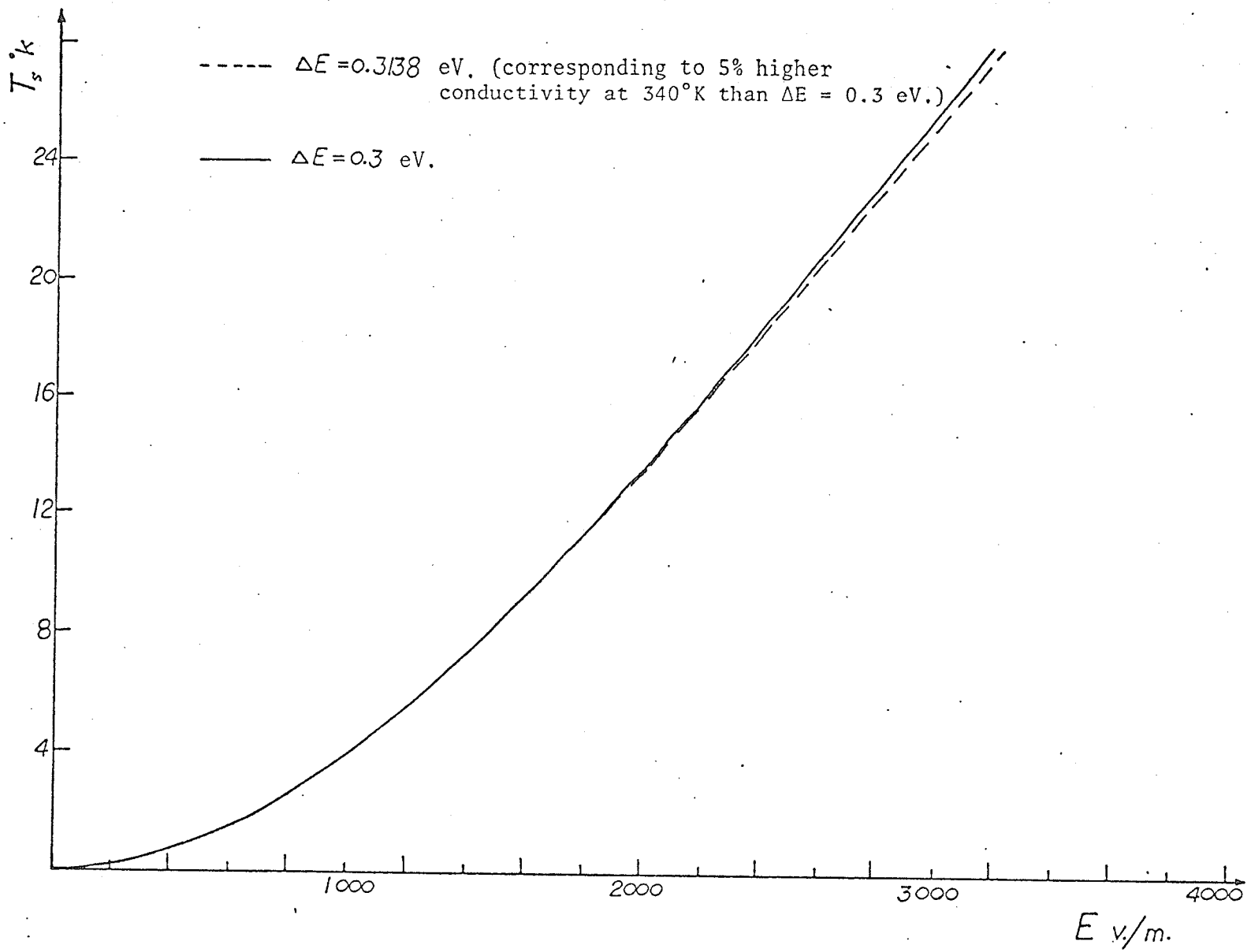

Fig. 4.5 Surface temperature (above 300°K) versus incident field with the conductivity as a parameter ($\omega = 10^{10}$ rad./sec.).

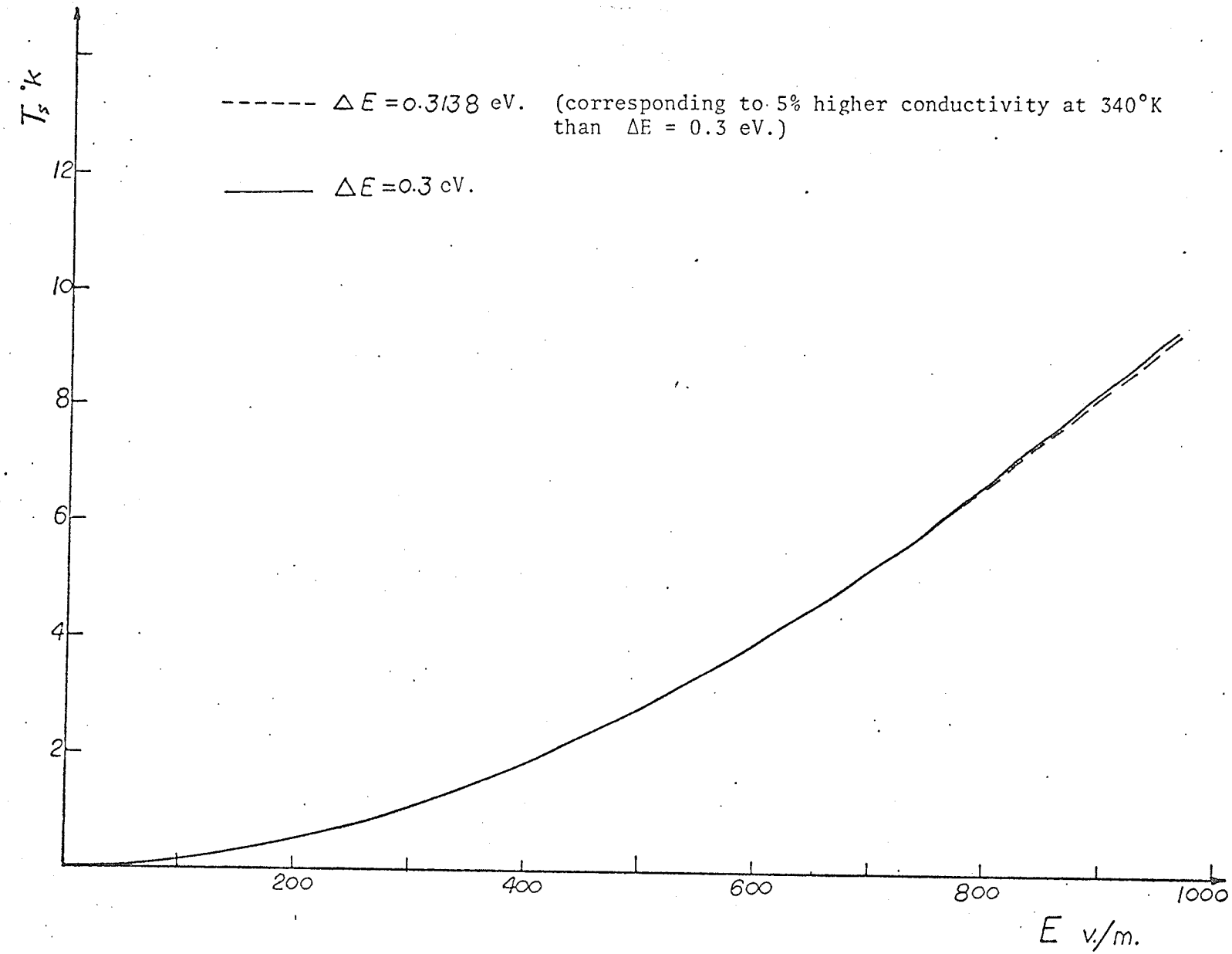

Fig. 4.6 Surface temperature (above 300°K) versus incident field with the conductivity as a parameter ($\omega = 10^{11}$ rad./sec.).

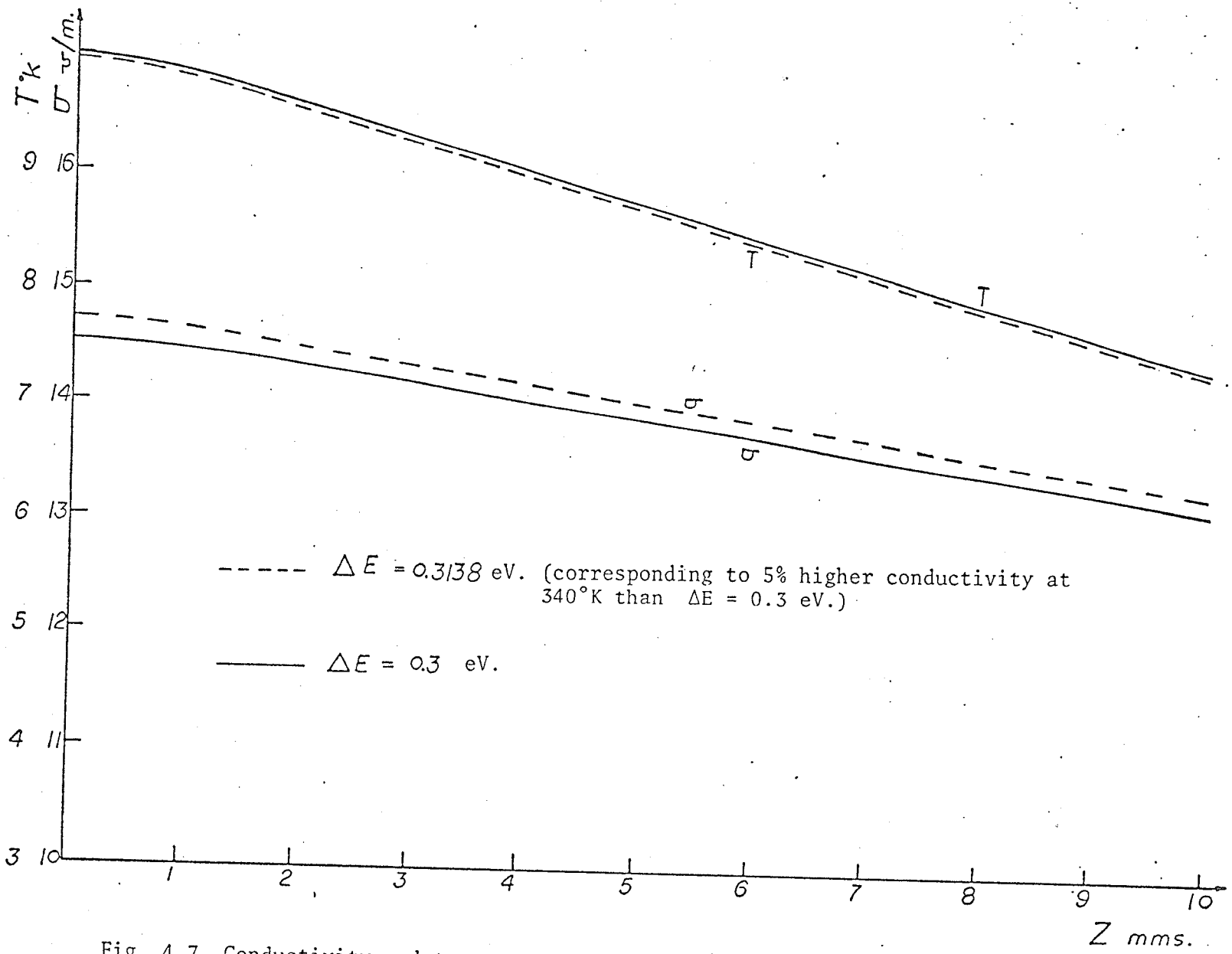

Fig. 4.7 Conductivity and temperature (above 300°K) versus distance inside the slab with the conductivity as a parameter (E^i = 1000.0 V·/m· and $\omega = 10^{11}$ rad./sec.).

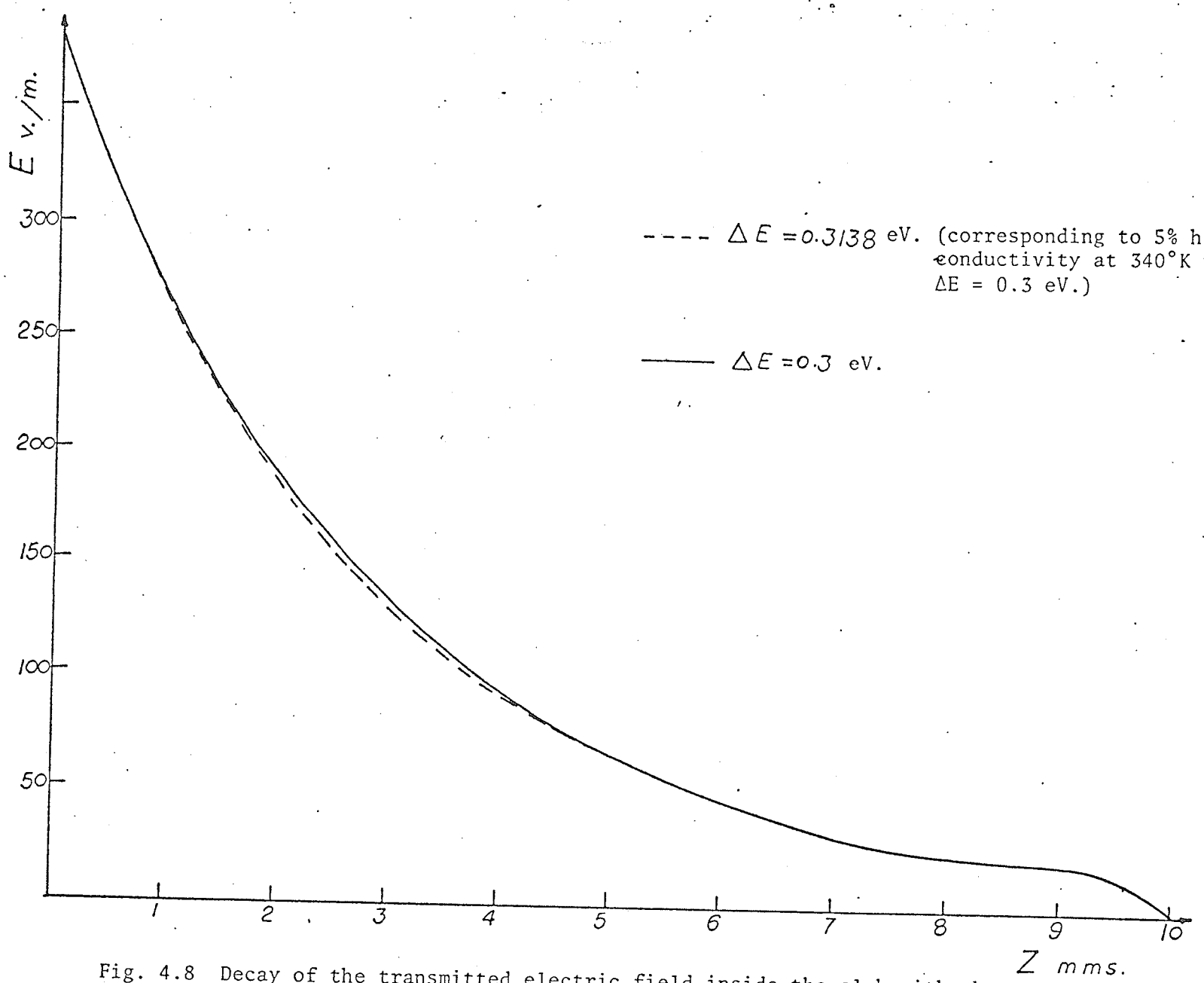

Fig. 4.8 Decay of the transmitted electric field inside the slab with the conductivity as a parameter (E^i = 1000.0 V•/m• and $\omega = 10^{11}$ rad./sec.).

relatively small amount of barium titanate. In doping VO_2 material with such dielectric, one has to worry about two factors: First, the thermal time constant of the composite material before the semiconductor becomes a metal and stops absorption of energy, second factor is the convergence of the subsequent cycle resulting from lesser power absorbed when the VO_2 conducts (or switches) which results in cooling leading to a tend to the semiconductor state. . . . . etc. The analysis of this process should prove interesting for a future investigation.

The variation of the surface impedance in a predictable manner [Figs. (3.7) to (3.9)] could also be a very efficient tool in numerous control and protection systems by using it as a variable load impedance to control the power flow in certain path in a lumped or printed microwave circuit. A proposal related to this type of application is given in Appendix E.

It is worth mentioning that the study of nonlinear interaction between electric and thermal properties of materials is not only restricted to transition-metal polyconductor, but it arises in several other cases especially where electromagnetic drying process takes place, such as microwave control of insect infestation and moisture content of grain, or the propagation of electromagnetic waves over the surface of wet soil heated by the sun. It is known that humid material lose high percentages of their water content if heated, hence their dielectric constant and conductivity change by a considerable factor. These problems can be dealt with using techniques similar to those developed in this thesis. Voss presented the power penetration depth [defined by the distance away from the surface at which the field drops by 36.8%

of its surface ($z = 0^+$) value] and the reflection coefficient at microwave frequencies for several values of ε_r' and ε_r'' [23]. However, he varied them in steps and considered their values to be constant at each step and not a function of the power. Thus suggests that Voss's analysis can be repeated more accurately taken the nonlinear nature of this problem into account.

5. SUGGESTED APPLICATIONS FOR FUTURE RESEARCH

A number of interesting applications have arisen during the course of this investigation. Since it was shown that the material changes its characteristics in a predictable manner, according to the frequency and intensity of the incident field, numerous applications and novel techniques in microwaves, especially in the field of instrumentations become apparent.

One problem which is always of constant interest is the measurement of microwave power for applications in microwave oscillators, microwave ovens, radar systems . . . etc. In most cases, measurements are accomplished by the use of a suitable calibrated thermal power detector or thermistor. Of basic importance of thermistors is the linearity between the power impressed and the temperature rise. Non thermal power detectors are also utilized, but they are generally less sensitive than the thermal detectors [22]. The VO_2 polyconductor slab, assuming that its resistivity-temperature exponential relationship holds at microwave frequencies, suggests an efficient and most sensitive thermal device for microwave power measurements, particularly at low power levels and especially if suitably biased so that the operating point lies on the part of the resistivity-temperature curve that has maximum slope. The analysis of a directional coupler proposed along these lines is given in Appendix D.

Another application is to use a VO_2 slab as a switching circuit element where connecting and disconnecting of a load is achieved by the power level impressed on a slab in the feed side of the load. For instance, antenna arrays in a radar system need not be operating except during the presence of a detectable target. Hence, by using the variable

characteristics of the VO_2 polyconductor, switching an array from the stand by to the active mode and vice versa can be easily controlled. The analysis of a proposal along this line is given in Appendix E.

It is worth mentioning that throughout this work, steady state condition is assumed. This is quite reasonable since the period of the cycle at microwave frequencies is much less than the period of the thermal cycle (i.e. the period of repetitive heating and cooling). If the electromagnetic field frequency is low or if the thermal cycle is rapid (such as the case if the operating point lies on the maximum slope of the conductivity - temperature curve) so that their periods are comparable, more complicated analysis where the time factor would no longer be neglected seems to be necessary.

APPENDIX A

Derivation of Equation (2.16)

It has been shown in section (2.2) that the conductivity may be expressed in the form

$$\sigma(T) = \sigma_o \exp(-F/T_K) \tag{A.1}$$

hence, at any reference temperature T_a, equation (A.1) becomes

$$\sigma(T_a) = \sigma_o \exp(-F/T_a) \tag{A.2}$$

Therefore

$$\sigma_o = \sigma(T_a) \exp(F/T_a) \tag{A.3}$$

Substituting (A.3) in (A.4) we obtain

$$\begin{aligned}\sigma(T) &= \sigma(T_a) \exp\left(\frac{F}{T_a} - \frac{F}{T_K}\right) \\ &= \sigma(T_a) \exp\left\{\frac{F}{T_a}\left(\frac{T_K - T_a}{T_K}\right)\right\}\end{aligned} \tag{A.4}$$

Letting $T_K = T_a + T$, where T is the temperature rise above the reference temperature, equation (A.4) becomes

$$\begin{aligned}\sigma(T) &= \sigma(T_a) \exp\left\{\frac{F}{T_a^2}\left(\frac{T}{1 + T/T_a}\right)\right\} \\ &= \sigma(T_a) \exp\{\beta\, T/(1 + T/T_a)\}\end{aligned} \tag{A.5}$$

APPENDIX B

Validity of Derivation of equation (3.6)

It could be shown that the sufficient condition for the second order differential equation (3.1) to have a solution in the form (3.2) is [20]

$$\frac{d\ f(z)}{d\ z} \Big/ [f(z)]^{3/2} << 1 \qquad (B.1)$$

hence, for the solution of equation (2.17) to be valid, the necessary condition (B.1) for the appropriate function $f(z)$ must be satisfied. Using equations (3.7), and (3.29), it is simple to show that this condition turns to be

$$\left| \frac{df(z)}{dz} \Big/ [f(z)]^{3/2} \right| = [\omega\mu\sigma(T_a)\ \exp\{\beta T/(1 + T/T_a)\} \cdot \frac{\beta}{(1 + T/T_a)^2} \cdot \frac{dT}{dz}]$$

$$/\ [(k_o^2\ \varepsilon_r')^2 + \omega^2\mu^2(\sigma(T_a)\ \exp\{\beta T/(1 + T/T_a)\} + \omega\varepsilon_o\varepsilon_r'')^2]^{3/2} \qquad (B.2)$$

From physical reasoning, a large variation of T with respect to z may be considered at the upper surface of the polyconductor where a sharp thermal discontinuity takes place. Hence, by virtue of equation (3.31), equation (B.3) may be written as

$$\left| \frac{df(z)}{dz} \Big/ f^{3/2}(z) \right| = [\omega\mu\sigma(T_a)\ \exp\{\beta T/(1 + T/T_a)\} \frac{\beta}{(1 + T/T_a)^2} \cdot 4\delta\varepsilon \frac{T_a^3}{k_a} T_S]$$

$$/\ [(k_o^2\ \varepsilon_r')^2 + \omega^2\mu^2(\sigma(T_a)\ \exp\{\beta T/(1 + T/T_a)\} + \omega\varepsilon_o\varepsilon_r'')^2]^{3/2} \qquad (B.3)$$

For the parameters used, it may be shown that

$$\omega\mu\sigma(T_a)\ \exp\{\beta T/(1 + T/T_a)\} >> \omega\ \varepsilon_o\varepsilon_r'' \qquad (B.4)$$

therefore, the term $\omega\ \varepsilon_o\varepsilon_r''$ can be dropped from the denominator of (B.3). It could be shown also that the L.H.S. of (B.4) is for the parameters used, greater than the quantity $k_o^2\ \varepsilon_r'$. Hence using the binomail theorem, (B.3) can be expressed as

$$\left|\frac{df(z)}{dz} / f^{3/2}(z)\right| \approx [\omega\mu\sigma(T_a)\ \exp\{\beta T/(1 + T/T_a)\} \cdot \frac{\beta}{(1 + T/T_a)^2}\ \frac{4\delta\varepsilon\ T_a^3}{k_3} \cdot T_S|$$

$$[(\omega\mu\sigma(T_a)\ \exp\{\beta T/(1 + T/T_a)\})^{3/2} \cdot \{\ 1 + \frac{3}{4}[\frac{k_o^2\ \varepsilon_r'}{\omega\mu\sigma(T_a)\exp\{\beta T/(1+T/T_a)\}}]^2$$

$$+ \ldots .\ \}] \qquad (B.5)$$

From (B.5), it is obvious that $|\frac{\partial f(z)}{\partial z}/f^{3/2}(z)|$ satisfies the inequality

$$|\frac{df(z)}{dz}/f^{3/2}(z)| < |\omega\mu\sigma(T_a)\exp\{\beta T/(1 + T/T_a)\}\ \frac{\beta}{(1 + T/T_a)^2} \cdot \frac{4\delta\varepsilon\ T_a^3}{k_a} \cdot T_S]/$$

$$[\omega\mu\sigma(T_a)\ \exp\{\beta T/(1 + T/T_a)\}]^{3/2}$$

$$< \frac{\beta \cdot (\frac{4\delta\varepsilon T_a^3}{k_a}) \cdot T_S}{\sqrt{\omega\mu\sigma(T_a)} \cdot \exp\{\frac{\beta T}{2}\ (1 + T/T_a)\}} \qquad (B.6)$$

Introducing the numerical values of the constants used throughout (section 3.1.1.), it is simple to show the following values:

$\beta = 0.0388$ $\qquad (^\circ K)^{-1}$

$4\delta\varepsilon T_a^3/k_a = 1.24$ $\qquad m^{-1}$

and for the lowest test frequency $\omega = 10^{10}$ rad./sec. we have

$$\sqrt{\omega\mu\sigma(300)} = 200\sqrt{\pi} \qquad m^{-1}$$

Hence, by substituting the above numerical values in (B.6) we obtain

$$\left|\frac{df(z)}{dz} / f^{3/2}(z)\right| < 13.52 \times 10^{-5} T_S << 1$$

which is obviously much less than unity. Thus condition (B.1) holds, and the validity of the solution given by equation (3.6) is established.

APPENDIX C

Numerical Solution for Equation (2.26)

A network of grid points is first established throughout the region $0 \leq z \leq h$ as shown in Fig. (C.1). The grid spacing H is equal to h/N where N is any arbitrary integer.

To obtain the same order of accuracy everywhere we make the following approximations [24]:

i) First derivative (dT/dz)

The first derivative is replaced by the approximate expression

$$\frac{dT}{dz} = \{T(Z_i + H) - T(Z_i - H)\} / 2H$$

$$= (T_{i+1} - T_{i-1}) / 2H \qquad (C.1)$$

where

T_i = the temperature at point z_i

T_{i+1} = the temperature at point z_{i+1}

T_{i-1} = the temperature at point z_{i-1}

This representation introduces two new points exterior to the region of the function. We shall discuss this later in this Appendix.

ii) Second derivative (d^2T/dz^2)

The second derivative is replaced by the approximation

$$\frac{d^2T}{dz^2} = (T_{i+1} - 2T_i + T_{i-1}) / H^2 \qquad (C.2)$$

Replacement of the derivatives by equations (C.1) and (C.2) will ensure that the accuracy everywhere is of the order of H^2 [24].

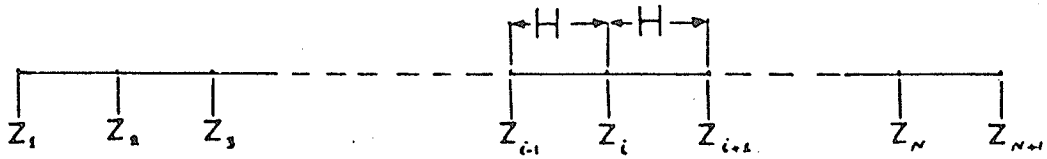

Fig. C.1 Grid points arrangement

Setting up the system of the above equations representing equation (2.26) in $N + 1$ points throughout region II $(0 \leq z \leq h)$, we obtain $N + 1$ simultaneous equations in $N + 1$ unknowns. These are the values of the temperature at each point of the network grid shown in Fig. (C.1).

Equation (2.26) is written for the $i^{\underline{th}}$ point as

$$(T_{i+1} - 2T_i + T_{i-1})/H^2 + \frac{1}{k_a}[\sigma(T_a)\exp\{\beta T_i/(1 + T_i/T_a)\} + \omega\,\varepsilon_o\varepsilon_r''] \cdot |E_i(z_i)|^2 = 0 \qquad i = 2, 3, \ldots N \tag{C.3}$$

where $|E_i(z_i)|$ is the magnitude of the electric field as given by equation (3.34). We notice that the range of 'i' is from '2 to N', it does not cover the two boundary points $i = 1$ and $i = N + 1$, since the substitution $i = 1$ and $i = N + 1$ in equation (C.3) results in two exterior points T_o at z_o and T_{N+2} at z_{N+2} respectively, which does not actually exist through the region of the function [See Fig. (C.1)]. To overcome the presence of these two points, use of the boundary conditions restrictions are made through equations (2.32) and (2.33) which govern the spatial rate of temperature variation at the upper and lower surfaces of the slab respectively. Equation (2.32) can be written in the form

$$\left.\frac{dT}{dz}\right|_{z=0} = 4\delta\varepsilon\, T_a^3\, T_S/k_a \tag{3.31}$$

making use of (C.1), (3.31) becomes

$$(T_2 - T_o)/2H = \frac{4\delta\varepsilon}{k_a} \cdot T_a^3 \cdot T_1$$

where it is clear that $T_1 = T_S$. This leads to

$$T_o = T_2 - \left(\frac{8\delta\varepsilon}{k_a} \cdot H \cdot T_a^3\right) T_S \qquad (C.4)$$

Putting $i = 1$ in (C.3) and using (C.4) gives

$$\left(2 + \frac{8\delta\varepsilon}{k_a} H \cdot T_a^3\right)T_1 - 2T_2 - \frac{H^2}{k_a}\left[\sigma(T_a)\exp\{\beta \cdot T_1/(1 + T_1/T_a)\} + \omega\,\varepsilon''\varepsilon_o\right] \cdot |E(0)|^2 = 0 \qquad (C.5)$$

Equation (C.5) is the first equation in the $N + 1$ set of equations. The $N + 1^{th}$ equation is readily obtained by reconsidering equation (C.3) at the point $N + 1$ where the electric field is zero. Hence, equation (C.3) becomes

$$T_{N+2} - 2T_{N+1} + T_N = 0 \qquad (C.6)$$

Again equation (2.33) is applicable at the point $N + 1$. Hence after making use of (C.6), equation (2.33) is readily shown to be

$$k_a(T_{N+2} - T_N)/2H + \frac{K_S}{S} T_{N+1} = 0$$

or alternatively

$$T_{N+2} = T_N - \frac{2 \cdot H \cdot K_S}{k_a S} \cdot T_{N+1} \qquad (C.7)$$

where T_h in equation (2.33) is replaced by T_{N+1}. Substituting (C.7) into (C.6) gives

$$T_{N+1} = T_N/(1 + HK_s/sK_a) \qquad (C.8)$$

which is the last of the set of $N + 1$ equations.

The complete set of the equations can be written now as

$$\left(2 + \frac{8H\delta\varepsilon}{k_a}\right)T_1 - 2T_2 - \frac{H^2}{k_a}\left[\sigma(T_a) \cdot \exp\{\beta T_1/(1 + T_1/T_a)\} + \omega\varepsilon_o\varepsilon_r''\right] |E_1|^2 = 0$$

$$2T_2 - T_3 - T_1 - \frac{H^2}{k_a}\left[\sigma(T_a) \cdot \exp\{\beta \cdot T_2/(1 + T_2/T_a)\} + \omega\varepsilon_o\varepsilon_r''\right] |E_2|^2 = 0$$

. . . . . .

. . . . . (C.9)

$$2T_N - T_{N+1} - T_{N-1} - \frac{H^2}{k_a}\left[\sigma(T_a) \exp\{\beta \cdot T_N/(1 + T_N/T_a)\} + \omega\varepsilon_o\varepsilon_r''\right] |E_N|^2 = 0$$

$$T_{N+1} - \frac{T_N}{(1 + HK_S/Sk_a)} = 0$$

An appropriate programme is set up to solve this set of equations simultaneously. The grid spacing H is taken as 1/10 millimter, hence (for the case of h = 1cm) the region $0 < z < h$ is divided into 101 points (i.e. N = 100) leading to a set of 101 simultaneous nonlinear equations in 101 unknowns. These are the values of the temperature at each point of the grid as given by the set (C.9).

Due to the nonlinear nature of these simultaneous equations, an iterative technique is employed, i.e. a solution for the temperature at every point throughout the grid is assumed then improved by successive iterations. To initiate a solution which is as close as possible to the correct one, the same problem is solved analytically but for constant conductivity, and the resulting values of the temperature are used to initiate the solution for the original problem. This method leads to a stable solution after only three iterations.

As a check on the accuracy of the results the solution for several selected cases are substituted back in the set (C.9) where the R.H.S of any of those equations must be zero. In all cases the error (defined as the value of the R.H.S.) is estimated around 10^{-4}. Typical results for the case of E^i = 1000 V/m. and $\omega = 10^{10}$ rad./sec. are presented in table (C.1 -p. 83) where it is shown that the maximum error is -1.59×10^{-4}. Also several cases are tested for smaller grid spacings (down to H = 1/50 mm) i.e. N = 500, where the same results are obtained.

APPENDIX D

Power Level Meter

It is possible to construct a power level meter by simply using a directional coupler and an impedance bridge to measure the conductance of the polyconductor slab which is connected as a load (thermally and electrically insulated from the walls) to the appropriate terminal of a cross guide directional coupler as shown in the diagramatic sketch (Fig. D.1). A matched generator is connected to terminal (1) while a matched load is connected to terminal (2) with the polyconductor slab loading terminal (3) and a known load connected to terminal (4). With this connection the power output of the generator as well as the power level at the known load [terminal (4)] could be determined.

Analytically the scattering matrix of the directional coupler is given by

$$[S] = \begin{bmatrix} 0 & A & 0 & jC \\ A & 0 & jC & 0 \\ 0 & jC & 0 & A \\ jC & 0 & A & 0 \end{bmatrix} \tag{D.1}$$

where A and C are known constants.

Introducing the power wave notations defined by [25]

$$a_i = \frac{1}{2}(V_i + I_i Z_o)$$

$$b_i = \frac{1}{2}(V_i - I_i Z_o) \tag{D.2}$$

where V_i and I_i are the voltage across and the current through the load Z_i, leads to the distribution of power wave components at each

terminal as shown in Fig. (D.2).

The relation between a_i and b_i is such that

$$R_i = b_i/a_i$$

where R_i is the reflection coefficient at the terminal load Z_i. Hence for a matched load b_i equals zero.

Since the power waves are linearly related to each other through the scattering matrix relation

$$[b] = [S]\,[a] \tag{D.3}$$

then for the connection of Fig. (D.1), using (D.1) equation (D.3) may be explicitly written as

$$\begin{bmatrix} b_1 \\ b_2 \\ b_3 \\ b_4 \end{bmatrix} = \begin{bmatrix} 0 & A & 0 & jC \\ A & 0 & jC & 0 \\ 0 & jC & 0 & A \\ jC & 0 & A & 0 \end{bmatrix} \begin{bmatrix} a_1 \\ 0 \\ R_3 b_3 \\ R_4 b_4 \end{bmatrix} \tag{D.4}$$

where a_3 and a_4 are replaced by $R_3 b_3$ and $R_4 b_4$, respectively.

From (D.4) we obtain

$$\begin{aligned} b_1 &= jC\, R_4 b_4 \\ b_2 &= A a_1 + jC\, R_3 b_3 \\ b_3 &= A\, R_4 b_4 \\ b_4 &= jC\, a_1 + A\, R_3 B_3 \end{aligned} \tag{D.5}$$

Hence, by monitoring the conductance of the VO_2 polyconductor load, R_3 as well as the power incident on it (a_3^2/Z_o) [25] are determined

from either calibrated curves or from the theoretical analysis given in Chapters 2 and 3. If the load reflection coefficient R_4 is known, the output power of the generator (a_1^2/Z_o) as well as the power incident on the load (b_4^2/Z_o) are completely determined from the set of equations (D.5).

It is important to notice that the waves inside the wave guide corresponding to the fundamental TE_{10} mode can be resolved into two plane waves propagating in different directions. Hence, the power incident on the VO_2 polyconductor will be due to two obliquely incident plane waves. Since our previous results are based on a single plane electromagnetic wave normally incident on the polyconductor surface, and since the problem is nonlinear, the effect of two plane waves can not be deduced from the analysis of a single plane wave. Therefore, if our previous results are to be employed, the VO_2 slab should be inclined in such a manner as to be normal to the direction of propagation of one plane wave and tangential to the other. Since the electric field is perpendicularly polarized, and the permeability of the polyconductor is the same as that of free space, no surface waves are launches [26]. It is simple to show that if the angle of inclination of the load with respect to the normal position is α, then

$$\sin \alpha = \lambda_o/2a$$

where λ_o is the free space wave length at the operating frequency, and a is the larger dimension of the wave guide cross section [see Fig. (D.3)].

The load inclination angle is obviously fixed at one frequency, however since the variation of $\sin \alpha$ is negligible for a small change

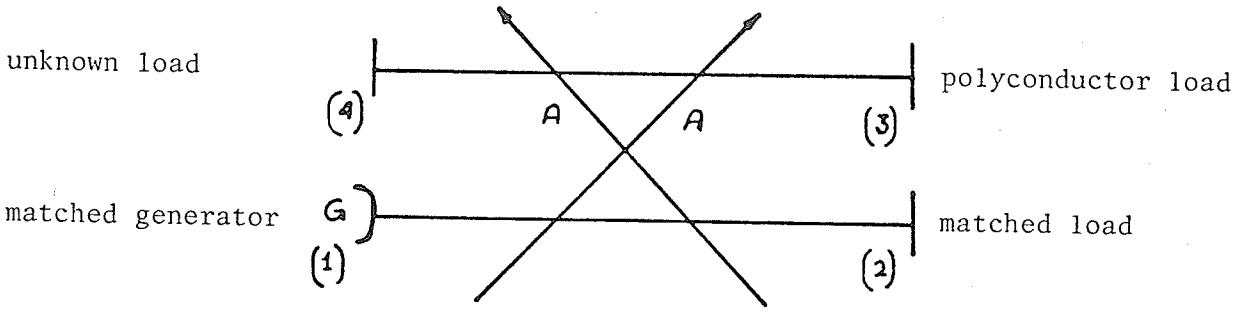

Fig. D.1 Diagramatic sketch of a power level meter.

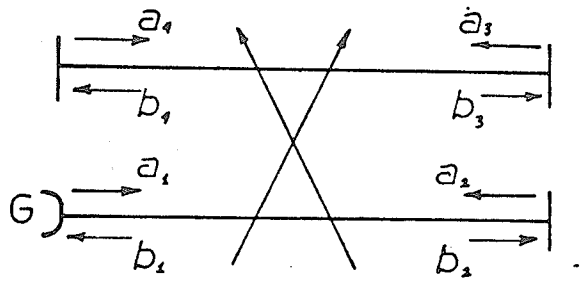

Fig. D.2 Power wave distribution at the terminals of the power level meter.

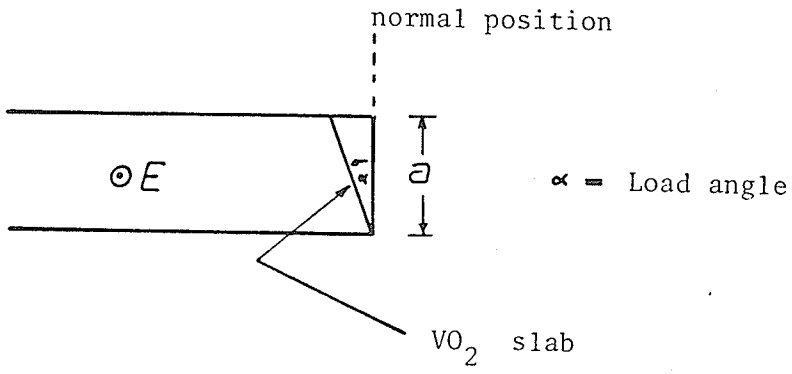

Fig. D.3 Load inclination in the power level meter.

in α, a kit of wave guides each having a fixed VO_2 load inclination adjusted to cover successive small frequency bands will serve to cover the whole band desired. To illustrate this assume a set of wave guides required to cover the frequency band 10 to 11 GHZ. A typical dimension of such a wave guide is 86 x 43 mm. Choosing the first element to cover the band 10 to 10.2 GHZ, the load inclination ranges from

$\alpha = 2°$ at 10GHZ to

$\alpha = 1° 58'$ at 10.2 GHZ, etc.

i.e., the load inclination can be considered constant over the limited frequency band at 10 to 10.2 GHZ.

APPENDIX E*

MOXI CONTROLLED ANTENNA ARRAY

An interesting application of the VO_2 slab on a metal substrate arises in radar systems where, as previously mentioned, switching of the standby array to the active mode is required only during the presence of a detectable target. The proposed connection is shown in Fig. (E.1). It consists of a wave guide directional coupler connected to the feed system of the surveillance antenna and terminated by a high power travelling wave tube (T.W.T.). The T.W.T. feeds a wave guide which acts as a parallel stub tuner to the second antenna and is blocked by a VO_2 film in series. The heater side of the film is on the T.W.T. side while the VO_2 variable impedance film on a very thin metal substrate is at end of the wave guide stub ($\lambda/4$ in length) as shown in Fig. (E.1). It is important to notice that the two antennas are electrically isolated (but not thermally) by the metal substrate.

In the normal state where one antenna is on surveillance and the other on standby, the VO_2 slab terminating the $\lambda/4$ parallel stub is at ambient temperature, hence, represents a very high input impedance Z_m. At the plane b-b [see Fig. (E.2)] the input impedance looking toward the stub Zi_{VO_2} is given by

$$Zi_{VO_2} = Z_o^2/Z_m \qquad (E.1)$$

where Z_o is the characteristic impedance of the wave guide for the TE_{1o} fundamental mode used.

---

* This appendix is related to a pending patent by Professor M.A.K. Hamid

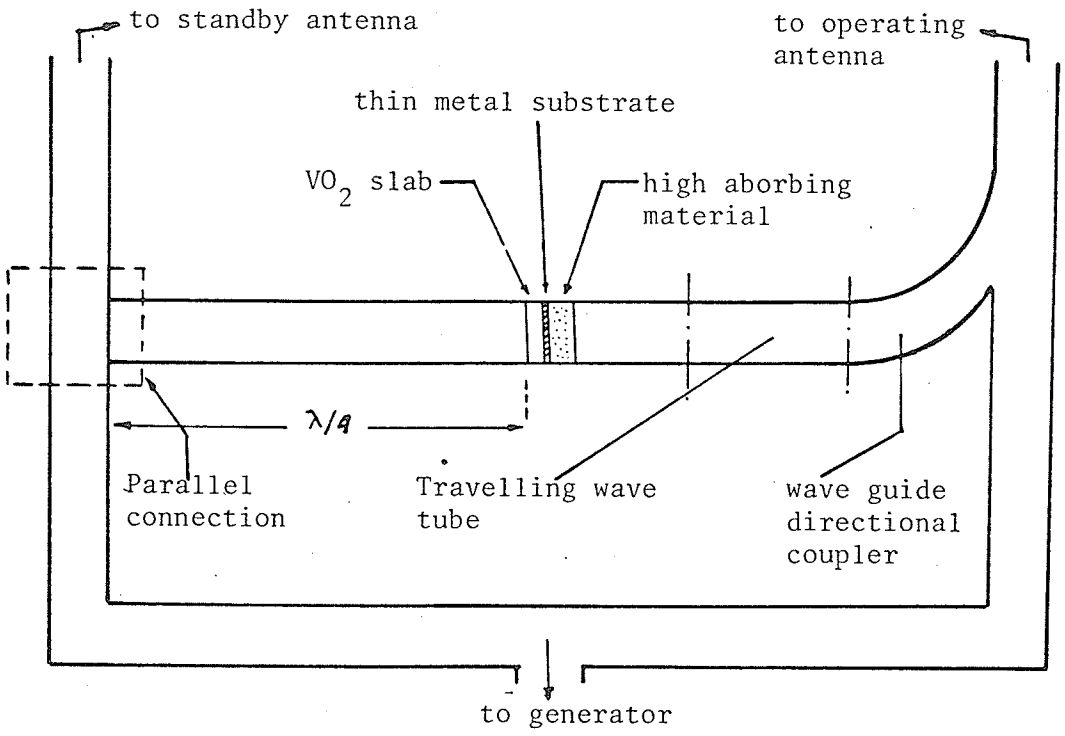

Fig. E.1 Moxi controlled antenna array.

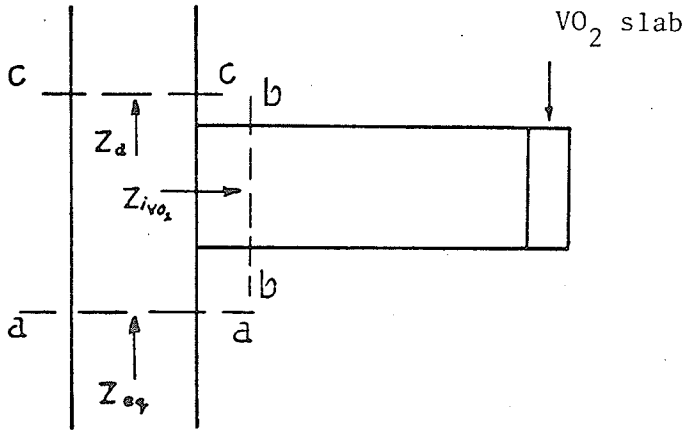

Fig. E.2 The parallel stub connection.

Let Z_a represent the input impedance of the standby antenna at plane C-C [Fig. (E.2)], therefore at plane a-a (same Figure) the equivalent input impedance Z_{eq} of the parallel combination of Z_a and Z_{iVO_2} is simply

$$Z_{eq} = (Z_a \cdot Z_{i_{VO_2}}) / Z_a + Z_{i_{VO_2}} \qquad (E.2)$$

Substituting (E.1) into (E.2) gives

$$Z_{eq} = Z_a \cdot Z_o^2 / [Z_{in}(Z_a + Z_o^2/Z_m)] \qquad (E.3)$$

Therefore, the impedance Z_{in} seen by the generator ($\lambda/4$ far from a-a) becomes

$$Z_{in} = Z_o^2/Z_{eq}$$

$$= Z_o^2 Z_m(Z_a + Z_o^2/Z_m) / Z_a Z_o^2$$

$$= Z_m + Z_o^2 / Z_a \qquad (E.4)$$

This value represents a very high impedance at the generator terminals, thus delivering negligible power to the standby antenna due to the resulting high standing wave ratio.

In the presence of a target, a back scattered signal is received, a sample of which will pass through the directional coupler to the T.W.T. where it is highly amplified, fed to the heater side of the film, thus causing a sudden rise in temperature. Hence heat transfer to the other side of the VO_2 film will take place immediately by conduction through the thin metal substrate. If the power transmitted is high enough to switch the VO_2, its impedance will drop sharply, and in effect it will turn to a metal which presents a short circuit termination to the quarter wave length parallel stub. Simple analysis will show that in this case Z_{iVO_2}

at the plane b-b will be infinite clearing the way for the generator to feed the standby antenna causing a sharper beam from the two antennas operating as an array. Once the target disappears, there will be no reflected signal to feed the T.W.T. and the VO_2 slab temperature will drop back to its normal condition causing the high impedance at the generator terminals to build up again and return the second antenna to the standby mode.

APPENDIX F

Scattering of plane electromagnetic waves from dielectric coated conductor- normal incidence

Consider an infinite dielectric sheet on a metal substrate as shown in Fig. (F.1). Let the dielectric sheet occupy region II ($0 < z < h$), the metal substrate occupy region III ($h < z < \infty$) and free space occupy region I ($z < 0$). Also assume a plane wave incident from region I normally on the slab with a y-polarized electric field given by

$$E^i = E_o \exp(-jK_o z) \tag{F.1}$$

where $\exp(j\omega t)$ time dependence has been suppressed.

The scattered field in region I is also a y-polarized and may be expressed in the form

$$E^s = R\, E_o \exp(jK_o z) \tag{F.2}$$

where R is the reflection coefficient at the surface $z = 0$.

At the interface between free space and the dielectric slab both the electric and magnetic fields are continuous, hence

$$E^i + E^s = E^t \tag{F.3}$$

$$H^i + H^s = H^t \tag{F.4}$$

where E^t is the transmitted electric field in medium II, H^i, H^s and H^t are the incident, scattered and transmitted magnetic field respectively.

Since from (2.6) we have

$$\frac{dE_y}{dz} = j\omega\mu\, H_x$$

then (F.3) and (F.4) can be written in the form

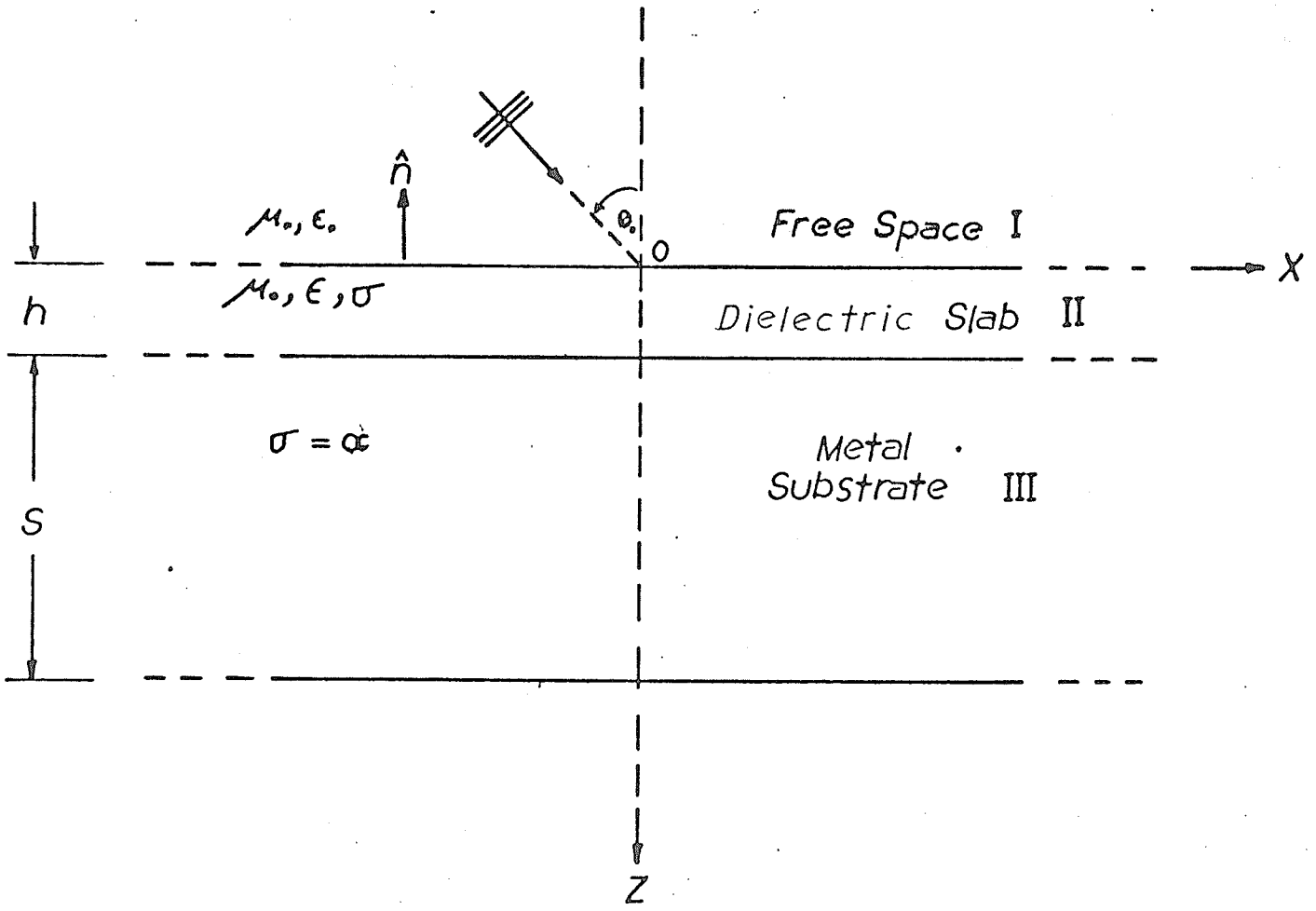

Fig. F.1 Scattering geometry for a dielectric coated conductor.

$$E_o(1 + R) = E^t \tag{F.5}$$

$$-\frac{jK_o}{j\omega\mu_o}(1 - R)\,E_o = \frac{1}{j\omega\mu}\left.\frac{dE^t}{dz}\right|_{z=0} \tag{F.6}$$

where μ is the permeability of the dielectric slab.

The electric field inside the dielectric must satisfy the wave equation

$$(\nabla^2 + K_d^2)E^t = 0 \tag{F.7}$$

where $K_d = \omega\sqrt{\mu\epsilon}$ is the dielectric wave number, ϵ is its permittivity. Since propagation is in z direction, equation (F.7) becomes

$$\frac{d^2E^t}{dz^2} + K_d^2\,E^t = 0$$

which has a solution in the form

$$E^t = A\exp(jK_dz) + B\exp(-jK_dz)$$

applying the electric field boundary condition at $z = h$ which requires that the total tangential electric field is zero gives

$$0 = A\exp(jK_dh) + B\exp(-jK_dh)$$

hence

$$E^t = A[\exp(jK_dz) - \exp(2jK_dH - jK_dz)].$$

$$= j\,2A\exp(jK_dh) \cdot \sin K_d(z - h) \tag{F.8}$$

Substituting (F.8) in (F.5) and (F.6) yields

$$E_o(1 + R) = -j\,2A\exp(jK_dh)\sin(K_dh) \tag{F.9}$$

and

$$-j \frac{K_o \mu}{\mu_o} (1 - R) E_o = j\, 2AK_d \exp(jK_d h) \cdot \cos(K_d h) \qquad (F.10)$$

Solving (F.9) and (F.10) simultaneously for A and R we get

$$R = \frac{1 - j \frac{K_o}{K_d} \cdot \frac{\mu}{\mu_o} \cdot \tan(K_d h)}{1 + j \frac{K_o \mu}{K_d \mu_o} \cdot \tan(K_d h)}$$

and

$$A = j\, E_o \exp(-jK_d h) \cdot \frac{\operatorname{Csc} K_d h}{1 + j \frac{K_o \mu}{K_d \mu_o} \cdot \tan(K_d h)} \qquad (F.11)$$

Substituting from (F.11) in (F.8) we finally obtain the transmitted electric field in the form

$$E^t = -2\, E_o \frac{\sin K_d (z-h)}{\left[1 + j \frac{K_o \mu}{K_d \mu_o} \tan(K_d h)\right]} \frac{1}{\sin(K_d h)} \qquad (F.12)$$

	TRANS. ELECT. FIELD	TEMP.	ERROR
1	0.142070471900 03	0.399125381CD 01	-0.211516294BD-04
2	0.159973674900 03	0.399125252900 01	-0.210597245500-04
3	0.157900907870 03	0.399067899740 01	-0.311707026400-04
4	0.155376555400 03	0.399055649220 01	-0.407162272600-04
5	0.153375979900 03	0.399059058030 01	-0.527259582620-04
6	0.151900724220 03	0.399057580960 01	-0.667798495700-04
7	0.149970224700 03	0.399213691CD 01	-0.740028715500-04
8	0.148064823900 03	0.399006613600 01	-0.834192002CD-04
9	0.146190927300 03	0.399568846700 01	-0.919484067300-04
10	0.144348430900 03	0.399266533500 01	-0.999335140600-04
11	0.142537219300 03	0.399837725400 01	-0.107031135500-03
12	0.140757179500 03	0.399372349100 01	-0.113694997400-03
13	0.139008184500 03	0.399872252200 01	-0.119576540D-03
14	0.137290103500 03	0.399339169700 01	-0.125026227300-03
15	0.135602788400 03	0.399477475950 01	-0.129870495100-03
16	0.133946081CD 03	0.399180585700 01	-0.134229066300-03
17	0.132319801900 03	0.399359133900 01	-0.138193855200-03
18	0.130723755300 03	0.399098812300 01	-0.141627291300-03
19	0.129157719900 03	0.399233952900 01	-0.144785509100-03
20	0.127621451800 03	0.399153492970 01	-0.147447366100-03
21	0.126114677680 03	0.399012623200 01	-0.149964695000-03
31	0.112583709400 03	0.398544290100 01	-0.159463549900-03
41	0.101395822100 03	0.398508835300 01	-0.165718012700-03
51	0.914994241560 02	0.398424053000 01	-0.139926209900-03
61	0.812958860020 02	0.398140722100 01	-0.119109012300-03
71	0.689651866700 02	0.398066525310 01	-0.901467006900-04
81	0.523063965500 02	0.398541104400 01	-0.540465186600-04
91	0.299447487700 02	0.398393396770 01	-0.182456946600-04

Table (C.1). Error for the case of E^i = 1000, w = 10^{10} rad./sec.

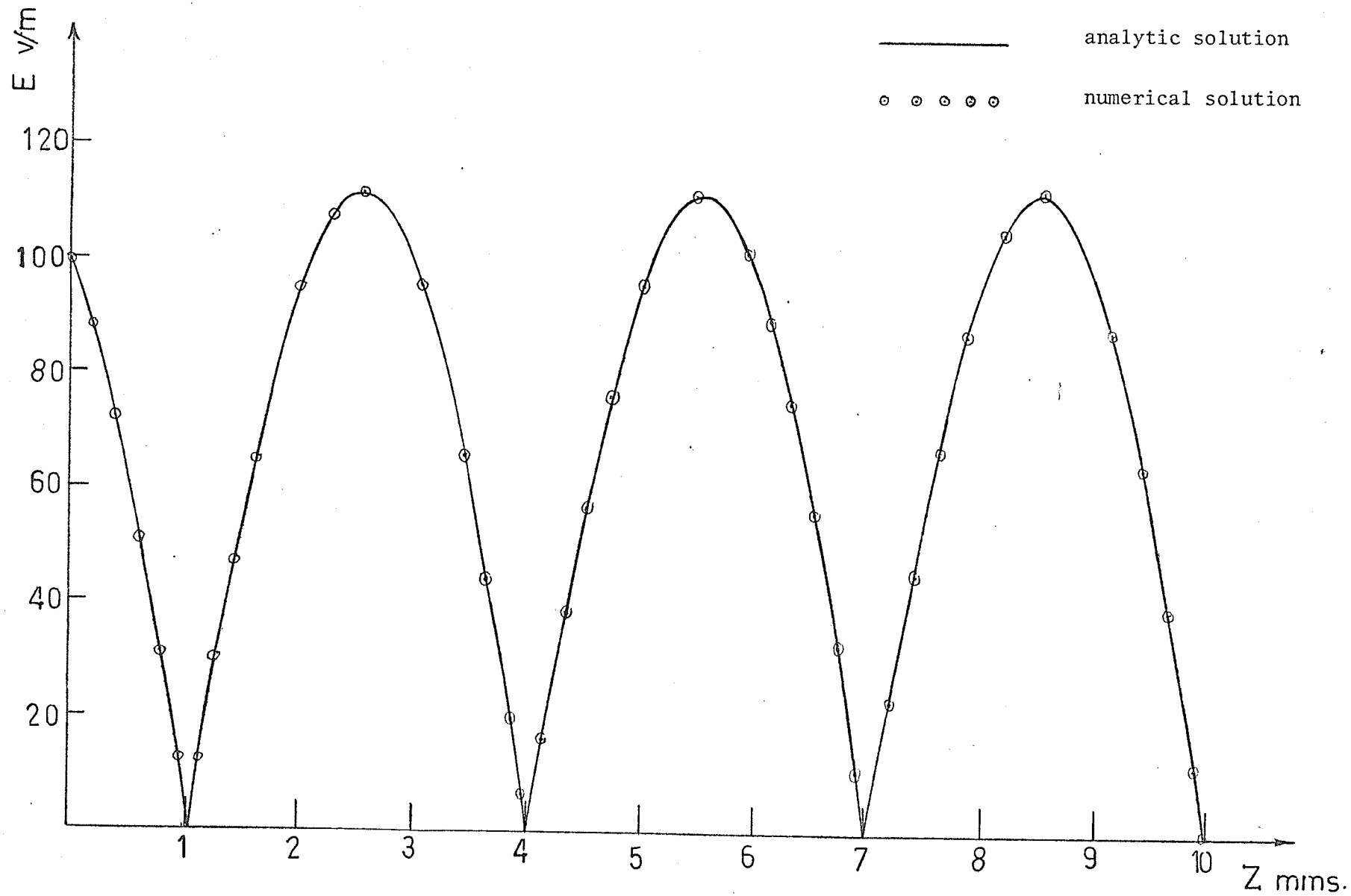

Fig. (F.2) Variation of the electric field inside the slab for the core of pure dielectric (both numerically and analytically) E^t = 100 v/m

BIBLIOGRAPHY

[1] R.J. Boulanger, W.M. Boerner, and M.A.K. Hamid, "Comparison of microwave and dielectric heating systems for the control of moisture content and insect infestations of grain," J. Microwave Power, Vol. 4, No. 3, pp. 194-208, Oct. 1969.

[2] J. Shmoys, "Long range propagation of low frequency radio waves between the earth and the ionosphere," Proc. I.R.E., Vol. 44, pp. 163-170, 1956.

[3] J. Galejs, "E.L.F. waves in the presence of exponential ionospheric conductivity profiles," I.R.E. Trans. on Antennas and Propagation, Vol. AP-9, pp. 554-562; Nov. 1961.

[4] J.R. Wait, Electromagnetic waves in stratified media. New York: Macmillan, 1962, Ch. 2.

[5] B.N. Lahiri and A.T. Price, "Electromagnetic induction in non-uniform conductors, and the determination of the conductivity of the earth from terrestrial magnetic variations," Phil. Trans. Roy. Soc., London, Ser. A, 237, pp. 507-540, 1939.

[6] C.T. Plough, "Canadian Moxie", Electron, p. 26, Nov. 1972.

[7] F.J. Morin, "Oxides which show a metal-to-insulator transition at the neel temperature," Phys. Rev. Lett., Vol. 3, pp. 34-36, 1959.

[8] D. Adler, "Mechanisms for metal-nonmetal transitions in transition-metal oxides and sulphides," Rev. Mod. Phys., Vol. 40, p. 714, 1968.

[9] W.D. Russel and C.H. Griffiths, "Moxie - a new device with answers to old problems," Internal report, Superior Elect. Indus. Limited, Montreal, Quebec.

[10] C.N. Berglund and H.J. Guggenheim, "Electronic properties of VO_2 near the semiconductor - metal transition," Phys. Rev., Vol. 185, p. 1022, 1969.

[11] C. Plough, "Polyconductivity," Rept. No. 4, DIR Project No. E159, Oct. to Dec. 1971, Ch. 4.

[12] A. Gavini and C.Y. Kwan, "Optical properties of semiconducting VO_2 films," Phys. Rev. B, Vol. 5, p. 3138, 1972.

[13] C.N. Berglund and R.H. Walden, "A thin film inductance using thermal filaments," IEEE Trans. Electron Devices, Vol. ED-17, pp. 137-148, Feb. 1970.

[14] J. Duchene, M. Terraillon, M. Pailly and G. Adam, "Initiation of switching in VO_2 coplanar devices," IEEE Trans. Electron Devices, Vol. ED-18, pp. 1151-1155, Dec. 1971.

[15] G. Adam and J. Duchene, "Pulse investigation of switching delays in VO_2 coplanar devices," IEEE Trans. Electron Devices, Vol. ED-19, pp. 820-825, June 1972.

[16] J. Duchene, M. Terraillon, M. Pailly and G. Adam, "Filamentary conduction in VO_2 coplanar thin-film devices," Appl. Phys. Lett., Vol. 9, p. 115, 1971.

[17] T.B. Senior, "Impedance boundary conditions for imperfectly conducting surfaces," Appl. Sci. Res., Sec. B, Vol. 8, pp. 418-436, 1961.

[18] H.S. Carslaw and J.C. Jaeger, Conduction of heat in solids. London, England: Oxford Press, 1959.

[19] R.F. Harrington, Time harmonic electromagnetic fields. New York: McGraw-Hill, 1961.

[20] F.H. Northover, Applied diffraction theory. New York: American Elsevier, 1971.

[21] B. Carnaham, H. Luther and J. Wilkes, Applied numerical methods. New York: John Wiley, 1969, Ch. 7.

[22] M. Sucher and J. Fox (Editors), Handbook of Microwave measurements, Vol. I. New York: Polytechnic Press, 1963.

[23] W.A. Voss, "Microwave instruments for material control. Part 1: A review," J. Microwave Power, Vol. 4, No. 3, pp. 210-216, Oct. 1969.

[24] S.D. Conte, Elementary numerical analysis. New York: McGraw-Hill, 1965.

[25] D.M. Kerns and R.W. Beatty, Basic theory of wave guide junctions and introductory microwave network analysis. Oxford, New York: Pergamon, 1967.

[26] J.A. Stratton, Electromagnetic Theory. New York: McGraw-Hill, 1941.